J Membrane Biol (2012) 245:29–50
DOI 10.1007/s00232-011-9413-3

Efficiency of Primary Saliva Secretion: An Analysis of Parameter Dependence in Dynamic Single-Cell and Acinus Models, with Application to Aquaporin Knockout Studies

Oliver J. Maclaren · James Sneyd · Edmund J. Crampin

Received: 24 February 2011 / Accepted: 15 December 2011 / Published online: 19 January 2012

Abstract Secretion from the salivary glands is driven by osmosis following the establishment of osmotic gradients between the lumen, the cell and the interstitium by active ion transport. We consider a dynamic model of osmotically driven primary saliva secretion and use singular perturbation approaches and scaling assumptions to reduce the model. Our analysis shows that isosmotic secretion is the most efficient secretion regime and that this holds for single isolated cells and for multiple cells assembled into an acinus. For typical parameter variations, we rule out any significant synergistic effect on total water secretion of an acinar arrangement of cells about a single shared lumen. Conditions for the attainment of isosmotic secretion are considered, and we derive an expression for how the concentration gradient between the interstitium and the lumen scales with water- and chloride-transport parameters. Aquaporin knockout studies are interpreted in the context of our analysis and further investigated using simulations of transport efficiency with different membrane water permeabilities. We conclude that recent claims that aquaporin knockout studies can be interpreted as evidence against a simple osmotic mechanism are not supported by our work. Many of the results that we obtain are independent of specific transporter details, and our analysis can be easily extended to apply to models that use other proposed ionic mechanisms of saliva secretion.

Keywords Fluid and electrolyte secretion in salivary glands · Epithelial transport · Mathematical modeling · Efficiency · Aquaporin

Introduction

Appropriate control of salivary fluid secretion is required for effective speech, mastication and general oral health. Salivary gland dysfunction affects a significant number of people (around 20% in the United States) and is often a consequence of certain medications or irradiation therapy, as well as being associated with diseases such as cystic fibrosis and Sjögren syndrome. Dysfunction can lead to oral pain, dental cavities and infections, as well as difficulties with eating and speaking.

Anatomically, there are three major pairs of salivary glands expressed in mammals: the parotid, submandibular and sublingual glands. These glands are primarily composed of two epithelial cell types—the acinar cells, which are arranged in clusters around a lumenal space forming the acini responsible for the secretion of salivary fluid and most salivary proteins, and the ductal cells, which modify

Electronic supplementary material The online version of this article (doi:10.1007/s00232-011-9413-3) contains supplementary material, which is available to authorized users.

O. J. Maclaren (✉) · E. J. Crampin
Auckland Bioengineering Institute, The University of Auckland, 70 Symonds Street, 1010 Auckland, New Zealand
e-mail: omac010@aucklanduni.ac.nz

J. Sneyd
Department of Mathematics, The University of Auckland, Auckland, New Zealand

E. J. Crampin (✉)
Department of Engineering Science, The University of Auckland, Auckland, New Zealand
e-mail: e.crampin@auckland.ac.nz

the composition of the saliva and secrete additional proteins as the saliva travels to the mouth. Most saliva secretion is due to the parotid and submandibular glands, with the parotid gland supplying the larger share.

Thaysen et al. (1954) proposed that saliva secretion is a two-stage process. The first step consists of the secretion of an isotonic, plasma-like primary fluid by the acini. This is followed by a modification of the ionic composition of this primary secretion by the ductal cells, during which there is little or no additional secretion or absorption of water. The final solution is then hypotonic by the time it enters the mouth.

A variety of ionic mechanisms have been proposed to account for the primary secretion by the acinar cells (see, e.g., Turner et al. 1993; Cook and Young 2010). Each of these mechanisms involves active ion transport, with ions taken up at one end of a cell and secreted at the other, establishing a transepithelial osmotic gradient which water follows. For two of the mechanisms discussed by Turner et al. (1993) and Cook and Young (2010), the secreted anion is chloride, while another involves the secretion of bicarbonate (the authors also discuss the experimental evidence for each of these processes). Rather than being strictly competing, it appears that a variety of processes act concurrently in the same gland, and possibly even in the same cell, to secrete fluid, with the relative importance varying over species, gland type and physiological condition. The chloride-based mechanism adopted in this report is thought to account for the majority of saliva secretion from the major salivary glands (Turner and Sugiya 2002).

Regardless of the particular ionic mechanism, the common feature of these explanations for fluid secretion is that salivary fluid flow is due to an osmotic gradient established between the lumenal region (surrounded by the acinar cells) and the intracellular space as well as between the intracellular space and the interstitium. This gives rise to a directed transcellular flow of water, from the interstitium into the intracellular region, then from the intracellular space into the lumen and out into the duct (see Fig. 1). The possibility of water moving via a paracellular pathway utilizing either the osmotic gradient between the lumen and the interstitium (established by the same mechanisms) or some alternative mechanism has also been much discussed in the literature on epithelial transport (Spring 1999; Hill et al. 2004; Hill 2008).

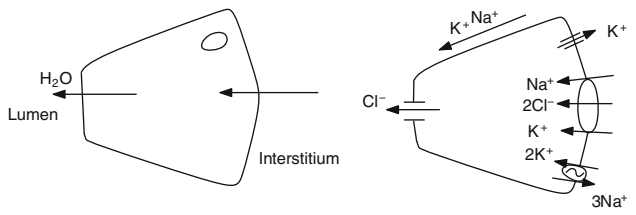

Fig. 1 Transcellular fluid secretion. *Left* direction of fluid flow. *Right* one mechanism, utilizing secretion of chloride, involved in fluid secretion

Notable models of osmotically driven fluid transport include the three-compartment model of Curran (1960) and the "standing-gradient" model of Diamond and Bossert (1967), both of which have been the basis of much of the work in this area. The primary motivation of the Curran (1960) model was to explain transport against an adverse osmotic gradient (between bathing solutions) by utilizing a middle coupling compartment bounded by membranes with differing solute and solvent-transport properties (Friedman 2008). Diamond (1964) criticized the ability of this model to represent isotonic transport, and this led to the development of the Diamond and Bossert (1967) model, which includes spatial gradients of concentration in the coupling compartment. Weinstein and Stephenson (1979, 1981a, b) emphasized that the issues of approximate isotonic transport and transport in the complete absence of, or against (uphill), osmotic gradients need to be distinguished and that each depends on a different combination of parameters. Of particular relevance here, Weinstein and Stephenson (1979, 1981a, b) recognized that the attainment of approximate isotonicity of transport depends essentially only on the cell membrane water permeability, which must be sufficiently high (while the ability to transport in the absence of, or against, an adverse osmotic gradient depends on restrictions of solute movement, e.g., via a basement membrane for absorptive epithelia and/or restricted diffusion in the relevant coupling compartment). Mathias and Wang (2005) considered a simple model of isotonic secretion and similarly demonstrated how small osmotic gradients between the cell and the compartments on either side of the cell which are close to, but not exactly, zero can produce near-isotonic fluid transport. Both sets of authors note that when the gradients are forced to be exactly zero, the secretion drops significantly and becomes much less isotonic.

As pointed out by a number of authors, models based on the standing-gradient model reduce in many cases to approximate mappings of the original compartment Curran (1960) model onto the appropriate physiological system (Weinstein and Stephenson 1981a; Spring 1999; Mathias and Wang 2005; Friedman 2008). Furthermore, although most models have been primarily concerned with fluid-absorbing epithelia, fluid secretion can also be understood using the basic conceptual scheme of the Curran (1960) model, as explained by Spring (1999). The resulting explanation of isotonic transport is thus given in terms of an osmotic coupling mechanism operating in the presence of small, but non-zero, gradients. This osmotic model is considered the "normal science" in epithelial transport (Schultz 2001); but as mentioned, this view has been and continues to

be criticized (Hill 2008; Fischbarg 2010), and many other mechanisms have been proposed for the process of fluid transport (e.g., Hill (2008) discusses various proposed mechanisms). In particular, Fischbarg (2010), Shachar-Hill and Hill (2002), Hill et al. (2004), and Hill (2008) have criticized the interpretation of aquaporin knockout studies, such as those of Ma et al. (1999), which are commonly used as support for the osmotic mechanism, and even suggest that aquaporins have gone from "saviors" of the osmotic theory to "its major problem" (Hill 2008). In the discussion we consider the results of aquaporin knockout studies and their various interpretations in the context of our analysis and simulations of a model of osmotically driven transcellular fluid flow. Furthermore, a common argument of those who accept the osmotic mechanism but reject the paracellular pathway is that the area of the tight junctions is too small to be permeable enough to admit a significant osmotic water flux (e.g., Spring (2010) offers a good discussion of this). In response to this, the main advocates of a paracellular water pathway tend to argue that a paracellular flux must be driven by nonosmotic mechanisms (Shachar-Hill and Hill 2002). Since we adopt the osmotic mechanism for this model, for consistency we initially ignore the paracellular route but come back to this in the discussion.

As discussed above, the modeling literature includes many primarily osmotically driven models of fluid transport, which have been analyzed by a number of authors, e.g., Weinstein and Stephenson (1979, 1981a, b) and Mathias and Wang (2005) (and both include aspects based on the earlier analysis of Segel (1970) of the Diamond and Bossert (1967) model). Both sets of authors utilize linearizations/perturbation expansions about the condition of isotonic/isosmotic transport and consider steady-state conditions. Our work takes a similar approach to analysis of the model behavior and conditions for (approximate) isotonic secretion. The main points of difference of our work are that (1) we focus on the problem of secretion into a small compartment, rather than the more common absorption from a small compartment (and into a larger bath); (2) we consider not only linearized/perturbation approximations to the model equations about the condition of isotonic/isosmotic secretion but also significant deviations from this state; and (3) our analysis applies directly to a (physiologically detailed) dynamic model, and hence, we work mostly in terms of scales and quasi-steady states as opposed to steady-state fluxes. In regard to point (1), while authors such as Weinstein and Stephenson (1979, 1981a, b) make reference to, and perform some calculations for, absorption from a mucosal (apical/lumenal) compartment into a small serosal (basal) compartment, which is an arrangement essentially equivalent to the secretion problem, they give more emphasis to the problem of absorption from a small mucosal bath into a large serosal bath. After linearization, these cases become more symmetric; but for larger deviations the interaction of the secretion into the small bath, convective removal from the bath and the concentration of the bath become important. Mathias and Wang (2005) gave more attention to this arrangement; however, they focused primarily on a perturbation solution to steady-state equations and applications to the renal proximal tubule. In regard to point (2), we only consider the standard linear phenomenological relationship for osmosis (described, e.g., in Schultz 1980); but we consider the effects of retaining nonlinear terms in the resulting model equations, in particular the term, discussed above, resulting from convective removal out of the lumen.

The model we consider is a physiologically based, dynamic, calcium-regulated model of primary saliva secretion, previously published by Gin et al. (2007), which consists of a system of nonlinear ordinary differential equations. Utilizing the approximation methods described above (scaling and singular perturbation methods) in combination with simulations of the full model, we explore fluid secretion as water permeability is decreased and secretion is no longer near the isotonic/isosmotic regime. This enables us to consider the consistency of the osmotic mechanism adopted here with aquaporin knockout studies such as those of Ma et al. (1999), in light of the criticisms by authors such as Hill et al. (2004) of the traditional interpretations of these studies.

Transcellular Fluid Secretion Model

Here, we consider a single-cell model based on Gin et al. (2007) for primary fluid secretion through a transcellular pathway. The ionic mechanism represented is that thought to be responsible for the bulk of the secretion in the major salivary glands (Turner and Sugiya 2002). In this model, the movement of Cl^- through the transcellular pathway, as well as the movement of Na^+ and K^+ via a paracellular pathway, sets up the required osmotic gradients between the three spaces. Based on the schematic model illustrated in the right panel of Fig. 1, we can write down the governing equations for conservation of ions and water volume. In what follows, the subscripts "e," "i" and "l" denote interstitial (extracellular), intracellular and lumenal compartments, respectively, which we assume to be well mixed. We do, however, allow a variable cell volume, w.

Cell Equations

The conservation of Cl^- ions in the intracellular region gives

$$\frac{\mathrm{d}([\mathrm{Cl}]_i w)}{\mathrm{d}t} = -\frac{I_{\mathrm{Cl}}}{z_{\mathrm{Cl}} F} + 2J_{\mathrm{NKCC}} \tag{1}$$

where F is the Faraday constant and $z_{\mathrm{Cl}} = -1$ is the valence of Cl^-. Here, Cl^- is brought into the cell via the Na^+–K^+–$2Cl^-$ cotransporter (J_{NKCC}) in the basolateral membrane, and efflux is via the apical Cl^- channel (I_{Cl}). The cotransporter moves two Cl^- ions for every K^+ and Na^+ ion. Similarly, conservation of Na^+ ions in the intracellular region gives

$$\frac{\mathrm{d}([\mathrm{Na}]_i w)}{\mathrm{d}t} = -3J_{\mathrm{NaK}} + J_{\mathrm{NKCC}} \tag{2}$$

Influx of Na^+ is due to the cotransporter, while efflux is due to the Na^+–K^+–ATPase (J_{NaK}), which pumps three Na^+ ions out for every two K^+ ions pumped in. Conservation of K^+ ions in the intracellular region gives

$$\frac{\mathrm{d}([\mathrm{K}]_i w)}{\mathrm{d}t} = 2J_{\mathrm{NaK}} + J_{\mathrm{NKCC}} - \frac{I_{\mathrm{K}}}{z_{\mathrm{K}} F} \tag{3}$$

These fluxes are due to the ATPase, the cotransporter and the K^+ channel (I_{K}) in the basolateral membrane.

Since we allow a variable cell volume, conservation of water in the intracellular region must be taken into account, giving

$$\frac{\mathrm{d}w}{\mathrm{d}t} = q_{\mathrm{b}} - q_{\mathrm{a}} \tag{4}$$

where

$$q_{\mathrm{a}} = R\Theta L_{\mathrm{pa}}(c_{\mathrm{l}} - c_{\mathrm{i}}) \tag{5}$$

$$q_{\mathrm{b}} = R\Theta L_{\mathrm{pb}}(c_{\mathrm{i}} - c_{\mathrm{e}}) \tag{6}$$

are the apical and basolateral water volume fluxes, respectively, and c_{e}, c_{i} and c_{l} are the total osmolyte concentrations in each region. L_{pa} and L_{pb} are the total water permeabilities of each membrane (area-weighted as in Gin et al. (2007), see Appendix A), R is the universal gas constant and Θ is the temperature. Note that the total intracellular concentration includes cell-impermeant X at concentration X/w and intracellular messengers such as Ca^{2+}.

Lumen Compartment

We assume that all external concentrations (composing c_{e}) surrounding the basolateral membrane remain unchanged; however, we allow variable lumenal concentrations. The lumenal region into which the primary secretion occurs is a small region surrounded by a spherical arrangement of acinar cells located in a secretory end piece (acinus). The primary secretion produced from the acinar cells then flows from the acinus lumen into a system of ducts of increasing size, beginning with the intercalated ducts. Due to the small dimensions of the lumenal region, we model this as well mixed. If we assume no volume change of the lumen and no pressure buildup, the water flux leaving the lumen is equal to q_{a}, the rate of secretion into the lumen. Furthermore, since the primary secretion is isotonic (in accordance with the two-stage hypothesis of Thaysen et al. 1954) and is pushed out as a combined bulk flow into the duct system, we assume that the removal of all ions, in particular Cl^-, from the lumen is dominated by convection by water. The second stage of transport, when the saliva is in the duct system, involves modification of the saliva composition along the duct length. However, here we model only the primary secretion from the secretory end pieces, and ductal transport and associated concentration changes are not considered further. This gives the lumenal Cl^- conservation equation

$$w_{\mathrm{l}} \frac{\mathrm{d}[\mathrm{Cl}]_{\mathrm{l}}}{\mathrm{d}t} = \frac{I_{\mathrm{Cl}}}{z_{\mathrm{Cl}} F} - q_{\mathrm{a}}[\mathrm{Cl}]_{\mathrm{l}} \tag{7}$$

where w_{l} is the lumenal volume surrounded by the acinar cells, which has an opening into the duct system.

Bicarbonate secretion is also thought to be involved in primary saliva secretion, although to a lesser extent than the chloride-based mechanism represented here (Turner and Sugiya 2002). It is not included in this model, and we briefly consider this assumption in the Discussion.

Voltage and Paracellular Ion Fluxes

In our model Na^+ and K^+ travel via the paracellular pathway, which are assumed to be cation-selective in accordance with the basic proposed mechanisms of saliva secretion (Cook and Young 2010). We consider the tight junction to be a simple membrane, with no ion–ion interactions. Furthermore, as discussed in the Introduction, we assume a fully transcellular pathway for water (and via an independent route—the aquaporins—to the chloride ions), so there is no convective transport. We return to these assumptions in the Discussion.

Assuming electrochemically driven fluxes, the K^+ tight junction flux could, e.g., be represented as

$$I^t_{\mathrm{K}} = g_{t,\mathrm{K}}(V_t - V_{\mathrm{K}}) \tag{8}$$

$$I^t_{\mathrm{Na}} = g_{t,\mathrm{Na}}(V_t - V_{\mathrm{Na}}) \tag{9}$$

where $g_{t,K}$, $g_{t,\mathrm{Na}}$, V_{K} and V_{Na} are the tight junction potassium and sodium conductances and Nernst potentials (between the interstitium and lumenal compartments), respectively, and V_t is the voltage difference between the lumen and interstitium.

Palk et al. (2010) discuss how to complete an electrophysiological model of this type, and they include differential equations for distinct apical and basolateral membrane

voltages. However, to good approximation (due to the small membrane capacitances), we replace these differential equations by electroneutrality constraints in each region. This is equivalent to taking a quasi-steady-state approximation of the differential equations, in which the voltage variables are slaved to the remaining variables. Based on these constraints, the total cation ion current ($I^t_{Na} + I^t_K$) must be such that it is equal to the total anion current (here, I_{Cl}).

$$I^t_{Na} + I^t_K = I_{Cl} \tag{10}$$

at all times. Given an initially electroneutral lumen, this implies

$$[Na]_l + [K]_l = [Cl]_l \tag{11}$$

Furthermore, when the lumenal fluid is approximately isotonic to the interstitium, the Nernst potential terms in (8) and (9) are negligible, and the currents are driven primarily by the same voltage difference. In this case, the relative amount of flux of Na^+ to K^+ is simply determined by the ratio of the respective conductances. Since the convective removal of a given ion from the lumen is proportional to its lumenal concentration and since $[K]_l \ll [Na]_l$. (from isotonicity we expect these concentrations to be close to their interstitial values), we would expect that $g_{t,K} \ll g_{t,Na}$.

The relative tight junction conductances are, in fact, not important here—the model behavior is independent of the actual proportion of cation current due sodium or potassium, respectively (other than in determining the proportions themselves, of course). Only (11) is actually required in the analysis that follows. For simplicity of simulation, we assume that the amount of potassium flux is such that the lumenal potassium concentration, $[K]_l$, is maintained at a value exactly equal to the interstitial potassium concentration, $[K]_e$ (noting that K^+ must be removed into the duct system along with the secreted fluid). This leaves the sodium flux as a variable to be determined by the electroneutrality constraint. These assumptions give

$$[K]_l = [K]_e \tag{12}$$

$$[Na]_l = [Cl]_l - [K]_l \tag{13}$$

though again we emphasize that, here, neither (12) nor (13) is required in the analysis that follows and the model results do not depend on either. Gin et al. (2007) used a constraint of electroneutrality between the lumen and the interstitium, i.e., $[Na]_l = [Na]_e - [Cl]_e + [Cl]_l$ instead of (13), which is in fact an equivalent assumption, given (12). Palk et al. (2010) considered the effects of adding a small apical potassium channel density, in which case the proportion of the cation concentration made up by sodium and potassium, respectively, does matter. This is beyond the scope of the present study, though extensions of our analysis are possible, e.g., by using assumptions on the potassium-to-sodium conductance ratio.

An electroneutrality constraint must also be specified for the cell compartment and, as for the lumenal region, this simply states that the fluxes of positive and negative charge must balance to give no net charge imbalance inside the cell. This allows the cell membrane voltage to be determined as an implicit function of the concentrations and volume, in terms of an equation of analogous form to (10). This equation also requires including calcium fluxes through the basolateral membrane (calcium signaling is discussed in the following section), and it is not required for the analysis that follows (though it is required in the full simulation model).

This completes our fluid flow model, without concern for the underlying details of channel/transporter activity and messenger dynamics. We can obtain some conclusions about this model irrespective of these details, while for full simulations and additional analysis we require explicit functional forms for these model aspects. The details used in that case follow Gin et al. (2007) and are briefly outlined in the next section. The full model equations and parameters are provided in the supplementary material.

Channels, Transporters and Signaling

The model we consider here is based on that of Gin et al. (2007). This model can conceptually be broken into two main parts—a three-compartment electrophysiological model of ion and water fluxes, which was described in the previous section, and a model of an oscillating calcium signal. We outline some of the properties of the model components here.

Ion and Water Transport

Here, we use the ion- and water-transport model of Gin et al. (2007, as detailed on pages 65–68, Tables 1–3 and the Appendices A and B).

Calcium-Dependent Channels

The ionic mechanism used in this model involves a Ca^{2+}-activated Cl^- channel in the apical membrane and a Ca^{2+}-activated K^+ channel in the basolateral membrane, in accordance with the literature (Turner et al. 1993; Cook and Young 2010). The steady-state open probability of the Cl^- channel is Ca^{2+}-dependent and includes voltage-dependent equilibrium constants. Gin et al. (2007) based this on a model developed for rat parotid acinar cells by Arreola et al. (1996). The K^+ channel open probability is Ca^{2+}-dependent but voltage-independent, in accordance

with the study of Takahata et al. (2003) on bovine parotid acinar cells.

ATPase

The model includes an Na^+–K^+–ATPase, which maintains low $[Na^+]$ and high $[K^+]$ in the cell, relative to the interstitium. It exchanges three Na^+ for two K^+ at the expenditure of ATP. Gin et al. (2007) used a reduced model by Smith and Crampin (2004), originally based on a model by Läuger and Apell (1986).

Cotransporter

The model includes a Na^+–K^+–$2Cl^-$ electroneutral cotransporter, a secondary active transport system which is the main uptake pathway for Cl^-. Gin et al. (2007) considered a 10-state scheme proposed by Lytle and McManus (1986) and formulated as a system of differential equations by Benjamin and Johnson (1997). They reduced this to a two-state model and then took the steady-state flux. We use this here.

Calcium Signaling Model

Here, we are primarily concerned with the ion and fluid transport, though under the influence of an oscillating Ca^{2+} signal. We are not as concerned with how the Ca^{2+} signal is generated. For this we refer to Palk et al. (2010), who describe modifications to the Gin et al. (2007) model. Our model has one slight difference again from the Palk et al. (2010) model, which is described in our Appendix B. Other than this, the signaling model is identical to that of Palk et al. (2010) and follows the details given in their article (see pp. 626–628 and Tables 1–3).

Analysis of a Single-Cell Model

The primary secretion formed in the lumen is known to be approximately isotonic to the source bath. This is usually viewed as being due to the relatively high water permeability for epithelial fluid transport (Turner and Sugiya 2002; Spring 1998). It is also known that the geometry of the acinus is such that the lumenal space is significantly smaller in volume than the acinar cells themselves. Here, we use the mathematical model to investigate the implications of these physiological observations.

Fluid Secretion and Scales

We first consider the equation governing the lumenal chloride concentration, $[Cl]_l$ (7), and the implications of a large water permeability (relative to other cell transport parameters) and a small lumen volume (relative to cell volume).

Estimate of Scale for Lumenal Concentration Increase

To begin, we will perform a scaling analysis and nondimensionalization of Eq. 7. Perspectives and case studies on scaling methods are offered in, e.g., Segel (1972), Segel and Slemrod (1989), Segel and Goldbeter (1994) and Krantz (2007). The results we obtain from this analysis will be compared in detail with simulations of the full model.

To be consistent with the requirement of (approximate) isotonicity of the secretion, the change in the lumenal concentrations must be small. In this model, the chloride current is the primary driver of the change in lumenal concentrations as the total cation ion concentration is determined by the lumen electroneutrality constraint (11). Thus, the change in total ion concentration in the lumen will be twice that of the chloride concentration, and both should be small for the model to reproduce expected results. In order to account for this in our scale for lumenal chloride concentration, we first define the new variable

$$[Cl]_{ld} = [Cl]_l - [Cl]_e \tag{14}$$

which represents the increase of $[Cl]_l$ above $[Cl]_e$. We now wish to define a scale for the change in $[Cl]_{ld}$ between stimulated and unstimulated conditions. We estimate this by considering the prestimulation steady state and poststimulation steady state of (7), without yet considering the dynamics in between or the effect of oscillations. Using (14), the steady-state relation obtained from (7) can be written as

$$\frac{I_{Cl}}{z_{Cl}F} = q_a\left([Cl]_{ld} + [Cl]_e\right) \tag{15}$$

To estimate the change in $[Cl]_{ld}$, we will assume for now that (15) holds both pre- and poststimulation, which we will denote by using a superscript "s" to indicate the poststimulation values ("stimulated") and a superscript "u" to represent the prestimulation values ("unstimulated"). Later, we will consider conditions for the steady state to hold during cell stimulation and an oscillating calcium signal, i.e., conditions for a quasi-steady state to hold for the actual variables (no superscript). Since $c_l - c_i < c_l - c_e = \Delta c$ and from electroneutrality $\Delta c = 2[Cl]_{ld}$, we can define a scale for the poststimulation fluid secretion rate as

$$q_a^s \sim 2R\Theta L_{pa}\delta \tag{16}$$

where δ is a scale parameter representing the maximum change in lumenal chloride concentrations (and is also a representative scale for total concentration changes since

these only differ by a factor of 2) and for which we will next determine an estimate in terms of the fluid- and chloride-transport parameters. Nondimensional quantities (represented by asterisks) can now be introduced for q_a^s, $[Cl]_{ld}^s$. and I_{Cl}^s, defined via

$$\begin{aligned} &[Cl]_{ld}^s = \delta [Cl]_{ld}^{s*}, \qquad I_{Cl}^s = \frac{z_{Cl} g_{Cl} R\Theta}{F} I_{Cl}^{s*}, \\ &q_a^s = 2R\Theta L_{pa} \delta q_a^{s*}; \end{aligned} \tag{17}$$

where g_{Cl} is a chloride conductivity parameter and δ is the chloride concentration change scale as defined above. The open probability of the chloride channel is typically much lower than 1—e.g., based on Palk et al. (2010) a value of around 0.1 is typical—hence, for simplicity of analysis, we take g_{Cl} to represent the product of the whole-cell chloride conductivity and the maximum open probability. Thus, for cells with identical physical characteristics, a higher g_{Cl} will represent a higher open probability, i.e., a higher stimulation level. We have also included the valency $z_{Cl} = -1$ in the nondimensionalization of I_{Cl} so that I_{Cl}^* is the magnitude of the chloride flux into the lumen. These scalings will ensure that the nondimensional poststimulation chloride current into the lumen and the poststimulation convective chloride removal out of the lumen have a nondimensional magnitude of about one. Using the same scalings for prestimulation values will mean that the resulting nondimensional values are small compared to one as we will assume that prestimulation values are at least an order of magnitude smaller than poststimulation values. Applying the steady-state equation to both cases and combining, we obtain

$$\begin{aligned} &\left(\frac{g_{Cl}}{(2L_{pa}[Cl]_e^2 F^2}\right)\left[I_{Cl}^{s*} + I_{Cl}^{u*}\right] = \left(\frac{\delta}{[Cl]_e}\right) \\ &\times \left[\frac{\delta}{[Cl]_e}\left(q_a^{s*}[Cl]_{ld}^{s*} + q_a^{u*}[Cl]_{ld}^{u*}\right) + \left(q_a^{s*} + q_a^{u*}\right)\right] \end{aligned} \tag{18}$$

By neglecting the nondimensional prestimulation values (setting to zero) and setting the nondimensional poststimulation terms to exactly one, we can obtain an estimate of δ, the scale of lumenal (chloride) concentration change. Solving (18) with these conditions (and taking the positive solution) gives

$$\frac{\delta}{[Cl]_e} = \frac{1}{2}\left(\sqrt{1+4\epsilon_d} - 1\right) = \epsilon_d - \epsilon_d^2 + 2\epsilon_d^3 + O(\epsilon_d^4) \tag{19}$$

where the series is derived from a binomial series (converging for $|\epsilon_d| < 1/4$), and we have defined

$$\epsilon_d \equiv \frac{g_{Cl}}{2L_{pa}[Cl]_e^2 F^2} \tag{20}$$

For $\epsilon_d \ll 1$, we see from the series expansion that

$$\frac{\delta}{[Cl]_e} \approx \epsilon_d \tag{21}$$

This will represent our scale under near-isotonic conditions. Note that this also represents the scale of total lumenal concentration change since $\frac{\delta}{[Cl]_e} = \frac{2\delta}{2[Cl]_e} = \frac{2\delta}{C_e} \sim \frac{\Delta C}{C_e}$. Considering this preliminary result, it is apparent that when the permeability is relatively large the fluid secretion term requires only very small differences in concentrations to balance the ion transport, and we obtain the isosmotic/isotonic case. This implies not only that isosmotic secretion requires large permeabilities (to generate enough fluid transport) but also that large permeabilities tend to produce isosmotic secretion. This is consistent with the conditions for iso-osmoticity given by Mathias and Wang (2005) (their Eq. 2) and Weinstein and Stephenson (1981b) (their Eq. 1-21). Later, we will consider the water permeability to be the main physical parameter controlling the size of these dimensionless groups since it is the large permeability of salivary cells (compared to other non-water-transporting cell types) that is most noteworthy. In addition to the near-isosmotic regime (ϵ_d, $\frac{\delta}{[Cl]_e} \ll 1$), we will consider how fluid secretion is affected when the ratio of chloride to water-transport parameters is no longer small, i.e., ϵ_d not negligible compared to 1, and hence significant osmotic gradients develop, i.e., $\frac{\delta}{[Cl]_e}$ no longer negligible compared to 1. Based on (19), we expect osmotic gradients ($\frac{\delta}{[Cl]_e}$) to grow more slowly than the ratio of transport parameters (ϵ_d).

Nondimensional Equation and Identification of Small Parameters

Returning to the main scaling analysis of (7) and considering (21), we can now introduce the following scalings, based on the isosmotic scales:

$$\begin{aligned} &[Cl]_{ld} = \frac{g_{Cl}}{2L_{pa}[Cl]_e F^2}[Cl]_{ld}^*, \quad I_{Cl} = \frac{z_{Cl} g_{Cl} R\Theta}{F} I_{Cl}^*, \\ &q_a = \frac{g_{Cl} R\Theta}{[Cl]_e F^2} q_a^*, \quad t = Tt^*; \end{aligned} \tag{22}$$

where T represents an as yet unspecified time scale of interest (the observation scale [Krantz 2007]), and the rest is consistent with the preceding analysis. As mentioned, the scale chosen for q_a is now fixed at the isosmotic scale, so q_a^* here will represent the ratio of q_a to its isosmotic value (which we will see is between 0 and 1). This scale is based on that of the poststimulation scale (16) combined with our scale for lumenal concentration changes in the limit of

$\epsilon_d \to 0$ (21). By first writing (7) in terms of $[Cl]_{ld}$ and then substituting the scalings (22) into the result, we obtain

$$\left(\frac{1}{T}\right)\left(\frac{w_l}{2R\Theta L_{pa}[Cl]_e}\right)\frac{d[Cl]^*_{ld}}{dt^*} = I^*_{Cl} - q^*_a\left(\frac{g_{Cl}}{2L_{pa}[Cl]^2_e F^2}[Cl]^*_{ld} + 1\right) \quad (23)$$

The term $\frac{w_l}{2R\Theta L_{pa}[Cl]_e}$ occurring on the left-hand side has dimensions of time, and we will call it T_t, taking it to represent a transient time scale. If this is small compared to our time scale of interest, i.e., $\frac{T_t}{T} \equiv \epsilon_t \ll 1$, then we obtain the singular problem

$$\epsilon_t \frac{d[Cl]^*_{ld}}{dt^*} = I^*_{Cl} - q^*_a\left(\epsilon_d[Cl]^*_{ld} + 1\right) \quad (24)$$

where $\epsilon_d \equiv \frac{g_{Cl}}{2L_{pa}[Cl]^2_e F^2} = \frac{\delta}{[Cl]_e} \sim \frac{\Delta c}{c_e}$, as before.

Time Scales of Interest

In order to determine under what circumstances we obtain the singular form (24), i.e., under what circumstances the condition $\frac{T_t}{T} \equiv \epsilon_t \ll 1$ holds, we need to consider what our time scale(s) of interest is.

We first use the equation for volume dynamics (4) to estimate the time scale over which significant changes in volume occur. Employing the same scaling for q_a and q_b as that used for q_a in (22), using $w = w_0 w^*$ to define the scaling of cell volume and $t = Tt^*$ for the time scale to be estimated, (4) becomes

$$\frac{w_0}{T}\frac{dw^*}{dt^*} = \frac{g_{Cl}R\Theta}{[Cl]_e F^2}(q^*_b - q^*_a) \quad (25)$$

During cell volume decrease, the volume flux out of the cell will dominate over the volume uptake. A balance of the left-hand side with the q_a term gives an estimate of the time scale for significant volume change. This can be achieved by setting $\frac{dw^*}{dt^*} = q^*_a = 1,\ q^*_b = 0$ and equating the scale factors, giving an estimate for the volume change time scale:

$$T_0 = \frac{w_0[Cl]_e F^2}{g_{Cl}R\Theta} \quad (26)$$

We can then use this time scale as our time scale of interest in (24), to obtain

$$(\epsilon_w)(\epsilon_d)\frac{d[Cl]^*_{ld}}{dt^*} = I^*_{Cl} - q^*_a\left(\epsilon_d[Cl]^*_{ld} + 1\right) \quad (27)$$

where $\epsilon_w \equiv \frac{w_l}{w_0}$ and $\epsilon_d \equiv \frac{g_{Cl}}{2L_{pa}[Cl]^2_e F^2}$ are each expected to be small under physiological conditions, due to the small lumenal volume (relative to cell volume) and the large water permeability (relative to chloride-transport parameters). Hence, we expect their product, ϵ_t, to be even smaller. This indicates a wide separation of scales, so we will assume (27) moves quickly (relative to the volume dynamics) to its quasi-steady state, given by

$$I^*_{Cl} - q^*_a\left(\epsilon_d[Cl]^*_{ld} + 1\right) = 0 \quad (28)$$

Since q_a increases/decreases with increases/decreases of $[Cl]_{ld}$, we expect sufficiently small perturbations of $[Cl]_{ld}$ (which leave I_{Cl} relatively unchanged, with any small changes in I_{Cl} expected to occur in the opposite direction) to return to the quasi-steady-state value. However, we do not consider the stability of the quasi-steady state in any more detail here. The equation of the steady state relating q_a and I_{Cl} will be exactly linear when $\epsilon_d \to 0$, while for small values (i.e., small deviations from iso-osmoticity) the relationship falls below this curve. The dependence of fluid secretion on chloride secretion is perhaps clearer if (28) is rewritten as

$$q^*_a = \left(1 - \epsilon_d[Cl]^*_{ld}\right)I^*_{Cl} \quad (29)$$

which is valid to first order for small ϵ_d (taking a Taylor series in ϵ_d). Hence, $q^*_a < I^*_{Cl}$ for nonzero ϵ_d and has the upper limit $q^*_a < I^*_{Cl}$ for $\epsilon_d \to 0$. This relationship will be discussed in detail later, and we also consider how it changes with non-negligible ϵ_d.

In order to consider the effects of an oscillating calcium signal, we need to consider another time scale of interest, a characteristic scale for the calcium spikes/oscillations. Based on the results of the models of Gin et al. (2007) and Palk et al. (2010) (which is the calcium signaling model used here), we estimate this to be about one to two orders of magnitude smaller than T_0 as given in (26), i.e., between $0.1T_0$ and $0.01T_0$. Using this scale in (27) instead of T_0 will still result in a singular equation as long as the product of ϵ_w and ϵ_d is sufficiently small, less than about 10^{-2}–10^{-3}. Based on typical parameter values used in later simulations, $\epsilon_w \approx \times 10^{-2}$, and $\epsilon_d \approx 10^{-3}$, up to a value of 1 for "low permeability" (relative to usual high values) ranges, giving a product of $\epsilon_t \approx 10^{-5}$ to 10^{-2}. This includes values of the desired order of smallness. However, as the permeability decreases, the system would be expected to still follow the general trend of the quasi-steady state on the time scale T_0 but may fail to fully follow the quasi-steady state exactly on the time scale of the calcium oscillations. The accuracy of the quasi-steady-state approximation will be tested by checking the correspondence to full simulations, and we will also consider consequences of any failure to exactly follow the oscillating quasi-steady state for low permeability values.

Cell Volume Quasi-Steady State

Although, as mentioned, the cell volume takes significantly longer to reach a new steady state after stimulation than the

lumenal concentrations, its steady state is still a useful tool for analysis. In particular, we will use it to obtain an approximation relating the fluid secretion to the change in total lumenal concentrations, which is independent of the internal cell concentrations. This will allow us to construct a good analytic approximation to the quasi-steady state of (27) relating q_a to I_{Cl} only, which captures the dependence on key parameters. The error in using the volume steady state for this purpose will be assessed in comparisons to simulations.

Expanding the expressions for q_a and q_b in (4) gives the quasi-steady-state condition for the volume ($q_a = q_b$) as

$$\frac{L_{pb}}{L_{pa}} = \frac{(c_l - c_i)}{(c_i - c_e)} \tag{30}$$

which can be rearranged to give an expression for c_i as a weighted average of c_l and c_e

$$c_i = \frac{L_{pa}c_l + L_{pb}c_e}{L_{pa} + L_{pb}} \tag{31}$$

when L_{pb} is greater than L_{pa}, the steady-state total osmolarity of the cell is closer to its initial value; and in the converse case, the steady-state total osmolarity of the cell is closer to that of the lumen. In either case the change is small. Since the net fluid secretion is equal to q_a, this gives an approximate expression for the fluid secreted:

$$q_a = R\Theta L_T(c_l - c_e), \tag{32}$$

where

$$L_T = \frac{L_{pa}L_{pb}}{L_{pa} + L_{pb}} \tag{33}$$

This expression for q_a is consistent with our previous scaling assumption for q_a. Using $c_l - c_e = 2([Cl]_l - [Cl]_e) = 2[Cl]_{ld}$ in (32) and using the result to eliminate $[Cl]^*_{ld}$ in the lumen quasi-steady-state relation (28) gives the quadratic relationship

$$\alpha q_a^{*2} + q_a^* - I^*_{Cl} = 0 \tag{34}$$

where $\alpha \equiv \left(\frac{g_{Cl}}{2L_T F^2 [Cl]_e^2}\right)$. The importance of the quadratic deviation from the linear approximation (the isosmotic case) is indicated by α, which measures the relative magnitudes of the chloride secretion and the fluid secretion and is proportional to $\epsilon_d = \frac{\delta}{[Cl]_e}$ (α has L_T instead of L_{pa}). We can use this expression to gain insight into the model, and we compare the accuracy of this approximation against simulations of the full model.

Efficiency of Secretion

Here, we consider the degree of deviations from the linear relationship between q_a^* and I^*_{Cl} arising from keeping the quadratic term in the quasi-steady-state relation (34). We can solve (34) for q_a^* in terms of I^*_{Cl}, giving

$$\begin{aligned} q_a^* &= \left(\frac{1}{\alpha}\right)\left(\frac{1}{2}\right)\left[\sqrt{1 + 4\alpha I^*_{Cl}} - 1\right] \\ &= I^*_{Cl}\left[1 - \alpha I^*_{Cl} + 2\alpha^2 I^*_{Cl}\right] + O(\alpha^3) \end{aligned} \tag{35}$$

which for $I^*_{Cl} = 1$ is

$$q_a^* = \left(\frac{1}{\alpha}\right)\left(\frac{1}{2}\right)\left[\sqrt{1 + 4\alpha} - 1\right] = 1 - \alpha + 2\alpha^2 + O(\alpha^3) \tag{36}$$

These series expansions illustrate the behavior for small α and converge for $\left|\alpha I^*_{Cl}\right| \leq 1/4$. Note also that the limits for $\alpha \to 0$ exist and are equal to 1. When α is non-negligible, we obtain the square-root relationship illustrated by the red line in panel 1 of Fig. 2, which is bounded by the linear, isosmotic limit. In the analysis here (and in following sections) we consider the difference between a system exactly following the linear form of the quasi-steady-state relation and the system exactly following the quadratic form of the quasi-steady-state relation. We include some consideration of deviations from quasi-steady state in comparisons to simulations, as well as later, in the discussion of aquaporin knockout studies.

This analysis demonstrates that for a given chloride current I_{Cl}, a larger L_T, i.e., a secretion closer to isosmotic, gives a larger fluid flow. The decrease in q_a^*, for a fixed chloride current (here, $I^*_{Cl} = 1$), as L_T is decreased is illustrated in panel 2 of Fig. 2. Starting from a small a value, e.g., 10^{-3}, L_T can be decreased by several orders of magnitude before changes in q_a^* become significant. As α approaches 1, we see that fluid flow drops to $1/\phi \approx 0.62\%$ of its isosmotic value (where ϕ is the golden ratio), for

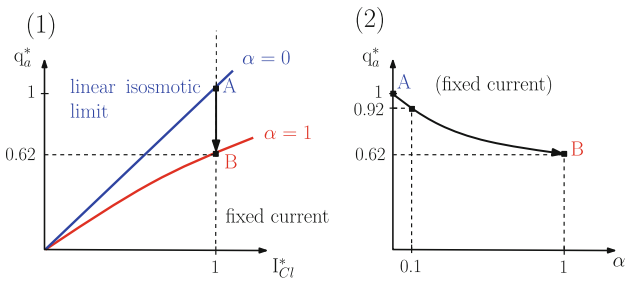

Fig. 2 Efficiency of fluid secretion. Two representations of the behavior of the solution (35) of the quasi-steady-state equation (34) relating fluid flow to chloride current for the large permeability limit (upper bound, *blue*) and finite permeability (*red*). The singular (large permeability, $\alpha = 0$) isosmotic case is an upper bound for fluid secretion and gives a greater flow at a fixed chloride current (1). For fixed chloride current, the dependence of fluid flow on the ratio (α) of the chloride and fluid transport parameters can be seen in *2*, while the change in shape of the whole solution is illustrated in *1*. For small α values, the decrease in fluid flow is roughly proportional, while the rate of decrease is lower for larger α values (Color figure online)

fixed chloride current. The chloride current is the main driver of the change in lumenal concentrations (electroneutrality or a similar constraint gives the concentration of the lumenal sodium), and maintaining this requires active processes operating at the basolateral end of the cell. Hence, we can consider (the isosmotic value of) I_{Cl} as a measure of the energy used in secretion. Since isosmotic secretion maximizes the flow for a given current, it is more efficient by this measure than nonisosmotic secretion at this same current. Although in this limit we are increasing the permeability L_T, we are also decreasing the concentration gradient available since the scale of the concentration difference is $\delta \propto 1/L_T$ (see the definition of α in Eq. 34). By this interpretation, panel 2 of Fig. 2 illustrates the change in fluid flow due to decreases in efficiency. Weinstein and Stephenson (1981b) and Hill and Hill (1978) defined similar measures of efficiency and coupling between solute and water fluxes in their studies of epithelial fluid transport. However, in their definitions of efficiency the authors required that the observed volume flow be that obtained for exactly equal bathing media. We do not make this restriction since we are interested in the volume flow observed for small but non-zero osmotic gradients.

The explanation for this maximal efficiency at isosmotic secretion lies in the natural balance between the transport of ions into the lumen and the removal of ions out of lumen, given in nondimensional form by (28). In this balance, the number of ions removed from the lumen per unit saliva is determined by the osmotic gradient, with a larger gradient giving a larger number of ions removed per unit saliva. When the total ion removal rate is constrained to balance a fixed ion current into the lumen, the largest fluid flow rate satisfying this is achieved when the number of ions removed per unit saliva is smallest; i.e., the osmotic gradient is smallest. As shown in the previous subsection, the size of the gradient, and hence the number of ions removed per unit saliva, is determined by the ratio of the chloride conductance g_{Cl} and the water permeability L_T.

Also of note is that once the permeability L_T is sufficiently large, and hence α is sufficiently small, the secretion is no longer dependent on L_T and is essentially proportional to the chloride current. Thus, the amount of fluid secreted under isosmotic conditions is less affected by variations in permeability than is nonisosmotic secretion. We will consider this feature more in the Discussion, in particular in the context of aquaporin knockout studies.

Numerical Simulations

We specify particular formulations for J_{NKCC}, J_{NaK}, I_{Cl} and I_K to complete the model discussed at a more general level thus far. These fluxes/currents depend on calcium signaling, IP_3 dynamics and voltage. For these dependencies, we follow Gin et al. (2007), with modifications described in our Appendix B. In these simulations none of the model approximations derived previously are used.

Baseline Behavior—Ion Concentrations and Volume

The basic behavior of the model is illustrated in Fig. 3. Following stimulation, chloride is secreted and the ion concentrations adjust to new levels, while the volume changes according to the secretion rate. The oscillations are due to the oscillatory nature of the calcium signaling (not shown).

The main intuitive features of the model response to stimulation are the increased calcium signal, which increases the open probability of the chloride channel and hence chloride flows from the cell, decreasing its concentration inside the cell; this decrease in chloride levels causes a compensating increase in the rate of chloride uptake via the cotransporter; this in turn increases the rate of sodium and potassium uptake via the cotransporter; the increase in cell sodium is offset by an increase in the ATPase pump rate; the increases in potassium uptake and pump rate are offset by the basolateral potassium channel, the open probability of which is also increased by the calcium increase.

Secretion, Efficiency and Variation in Permeabilities

Next we consider the question of efficiency and total secretion for varying permeabilities (Fig. 4). It can be seen that the quasi-steady-state expression relating fluid secretion (q_a) and chloride current (I_{Cl}) derived previously (34) accurately accounts for the changes in fluid flow for the different permeabilities. As expected, if the permeability is large (Fig. 4a), the linear quasi-steady-state approximation (the isosmotic limit) is sufficient to capture the behavior. As the permeability is decreased (Fig. 4b, c), the drop in secretion is accounted for simply and to reasonable accuracy by using the quadratic quasi-steady-state relation derived. Thus, the drop in fluid secretion is mainly due to a drop in efficiency (for bigger concentration gradients), the effect of which can be estimated by comparing, in each case, the linear approximation to the quadratic approximation (where the quadratic approximation closely follows the actual simulations). The difference in total secretion between the panels also includes a part due to a decrease in chloride current, which can be seen by the slight difference in the respective fluid flows as calculated from linear quasi-steady-state relation in each case. This decrease is also due to the inefficiency of an increase in lumenal concentrations since the stimulation levels remain the same, though the fixed-current drop in efficiency represents the dominant effect.

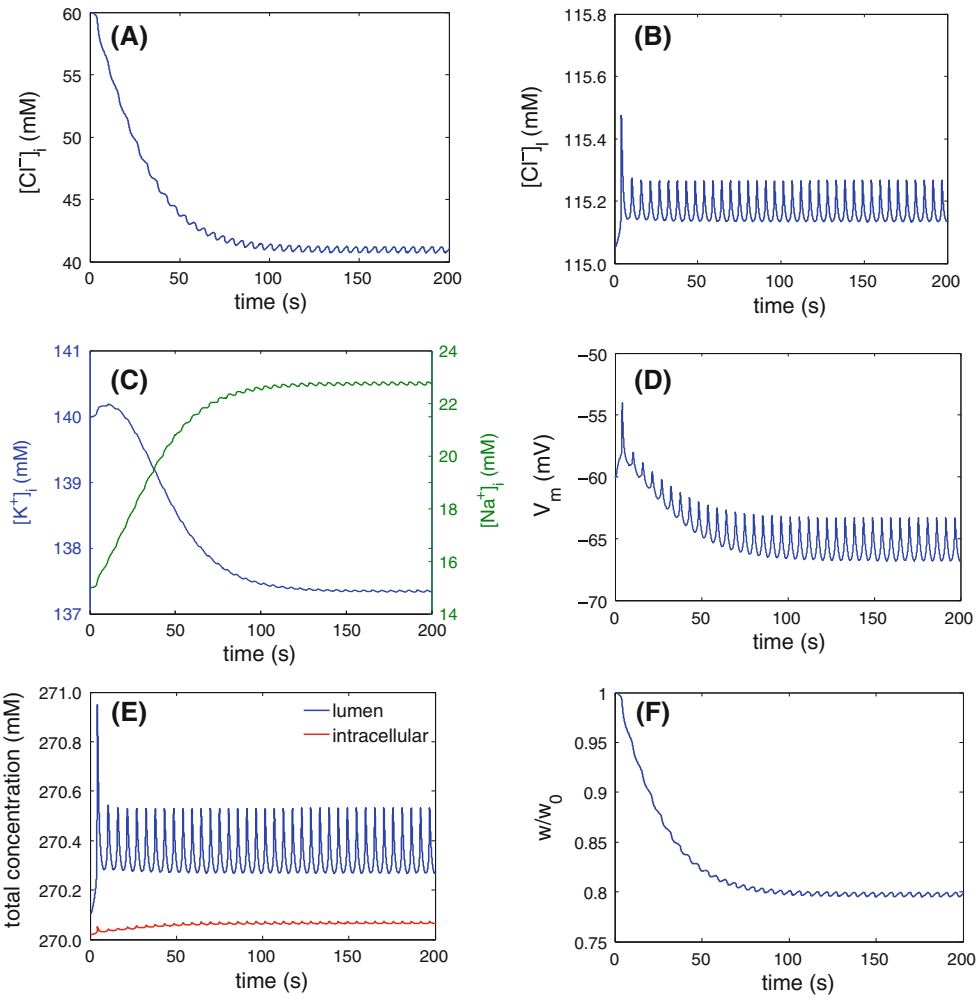

Fig. 3 Baseline behavior. There are oscillatory shifts to new levels for the ions ($[Cl]_i$, $[Na]_i$, $[K]_i$, $[Cl]_l$), membrane voltage, total concentrations and cell volume (**a**–**f**, respectively)

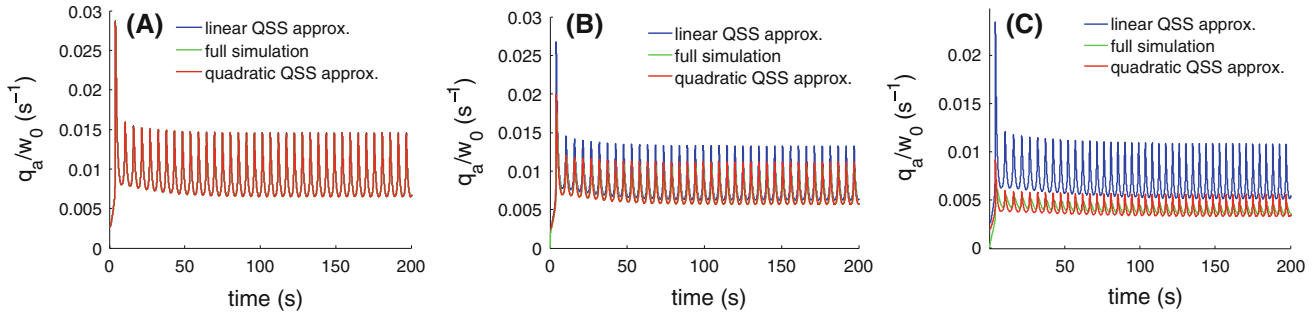

Fig. 4 Simulation plots of fluid secretion for a range of permeabilities. **a** $L_{pa} = 1.23 \times 10^{-14}$ L^2 J^{-1} s^{-1}. **b** $L_{pa} = 1.23 \times 10^{-16}$ L^2 J^{-1} s^{-1}. **c** $L_{pa} = 1.23 \times 10^{-17}$ L^2 J^{-1} s^{-1}. $L_{pb} = 4L_{pa}$ in all cases. In **a** all the traces are indistinguishable. As the permeability is decreased (**b**, **c**), the quadratic quasi-steady-state approximation follows the full simulation results, while the linear quasi-steady-state approximation overestimates the secretion, consistent with our prediction of it as an upper bound. In the lower-permeability range, the quadratic steady state slightly overestimates the true water-transport rate during rapid spikes

The accuracy of the lumenal chloride transport quasi-steady-state Eq. (28) decreases with decreasing permeability since the time for the lumen concentrations to reach their quasi-steady state depends on the size of the lumen changes (see 27). As the permeability decreases and the size of the lumenal concentration changes increase, the lumen does not reach the quasi-steady state as fast. This means that the convective chloride removal does not

increase fast enough to balance the fastest spikes in chloride current, and the quasi-steady state overestimates the actual chloride removal during these spikes. This deviation from the quasi-steady-state case represents another (dynamic) form of inefficiency and needs to be taken into account when considering any experimentally determined drop in salt secretion since it is the convective quantity that corresponds to what would be collected experimentally from inside (or at the end of) ducts. This will be discussed further in the context of aquaporin knockouts.

The derivation of the approximate quasi-steady-state Eq. (34), relating q_a and I_{Cl} directly, involved the use of the quasi-steady-state fluid secretion rate obtained from consideration of the volume Eq. (4), along with the assumption of a fast transition to the quasi-steady state of the lumenal chloride Eq. (7), given by (28). As discussed, the time for the volume to reach a quasi-steady state is much longer than for the lumenal concentrations. Since the size of the error depends on how close q_a is to its steady-state value during dynamic changes, the error depends on the relative size of the large, fast increase in q_a due to fast lumenal increases in concentration and the size of the smaller decrease in q_a due to slower increases in total cell concentrations. This error decreases on the slow time scale. Furthermore, the importance of this error is reduced due to the approximation being used in the term multiplied by the small parameter ϵ_d.

These errors account for the deviations of the approximation from the actual simulated values, although it still appears to give a good characterization of the model behavior. Additionally, we note that since the volume takes some time to reach a quasi-steady state and has slight variations about it, we cannot simply assume that the volume variable becomes slaved to others in the same way as we might for a truly singular equation. Computing the volume variable in this way underestimates the total volume decrease due to the initial larger flux of water from the apical membrane (calculations not shown). Instead, we must include the full volume differential Eq. (4).

Acinus Model—Lumenal Coupling

Above, we have discussed the efficiency of saliva secretion in a single cell; however, the main secretory unit of a salivary gland is an acinus end piece—a spherically arranged clump of cells surrounding a shared lumen. A simple schematic of a section through an acinus illustrating the arrangement of cells is given in Fig. 5. Secretions into the lumen are then pushed out into the duct system. The geometric arrangement of cells in an acinus leads to the possibility of coupling effects being induced via the (shared) NaCl concentration in the lumen.

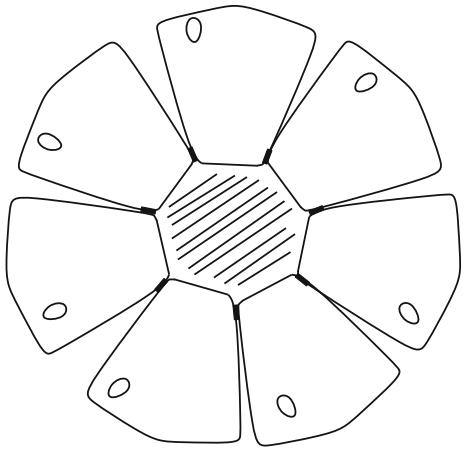

Fig. 5 Salivary acinus (not to scale). Cells are arranged about a shared lumenal region (*hatched*)

We model an acinus as an arrangement of n cells secreting into a single lumen by taking a copy of Eqs. 1–6 for each cell, giving for the jth cell:

$$\frac{d([Cl]_i^j w^j)}{dt} = -\frac{I_{Cl}^j([Cl]_l, \ldots)}{z_{Cl}F} + 2J_{NKCC}^j \tag{37}$$

$$\frac{d([Na]_i^j w^j)}{dt} = -3J_{NaK}^j + J_{NKCC}^j \tag{38}$$

$$\frac{d([K]_i^j w^j)}{dt} = 2J_{NaK}^j + J_{NKCC}^j - \frac{I_K^j}{z_K F} \tag{39}$$

$$\frac{dw^j}{dt} = q_b^j - q_a^j \tag{40}$$

Equation 7 for the lumenal chloride concentration, $[Cl]_l$, is modified to take into account the chloride flux from each cell, giving

$$w_l \frac{d[Cl]_l}{dt} = \frac{\sum_{i=1}^n I_{Cl}^i}{z_{Cl}F} - \left(\sum_{i=1}^n q_a^i\right)[Cl]_l \tag{41}$$

again assuming no pressure buildup in the lumen. Each cell is modeled in the same way, but we allow for different parameters and/or different constitutive equations as desired. Here, we will consider the results from identical cells with heterogeneous levels of cell stimulation (as would be expected from the spatial arrangement and separation of the cells), which manifests as a difference in the chloride currents, I_{cl}^j, for each cell $j = 1 \ldots n$.

Volume Quasi-Steady State

The analysis of the volume equation for a single cell can be immediately carried over to each cell in the acinus arrangement (though, as for a single cell, this quasi-steady-state assumption must be verified by simulation). In

particular, for each cell, the quasi-steady-state result (32), $q_a = R\Theta L_T(c_l - c_e)$, applies, i.e., for the jth cell:

$$q_a^j = R\Theta L_T^j(c_l - c_e) = 2R\Theta L_T^j[\mathrm{Cl}]_{ld} \tag{42}$$

where

$$L_T^j = \frac{L_{pa}^j L_{pb}^j}{L_{pa}^j + L_{pb}^j} \tag{43}$$

Since this expression depends only on the shared lumenal concentration and the homogeneous external environment, it follows that at the quasi-steady state, cells with the same water permeabilities secrete water at the same rate, even when the cells have different chloride (and sodium) secretion rates. This indicates that the coupling arising from the geometric arrangement leads to results that differ from what would be obtained from a collection of independent cells, in this case resulting in similar water secretions from differently stimulated cells.

Efficiency

Here, we extend the analysis of efficiency to the multicell case, yielding an analogous result for coupled cells, and consider the size of coupling effects.

Quasi-Steady State

Firstly, the (quasi-) steady state of (41) can be written as

$$\frac{\sum_{i=1}^n I_{Cl}^i}{z_{Cl}F} = (\sum_{i=1}^n q_a^i)([\mathrm{Cl}]_{ld} + [\mathrm{Cl}]_e) \tag{44}$$

which can be rewritten as

$$\frac{\bar{I}_{Cl}}{z_{Cl}F} = \bar{q}_a^c([\mathrm{Cl}]_{ld}^c + [\mathrm{Cl}]_e) \tag{45}$$

where we have used a superscript c to indicate coupled cell quantities (we do not include a superscript on $\bar{I}_{Cl}$ since we will be interested in fixed currents, regardless of coupling). Now (42) can be used to write

$$\bar{q}_a^c = 2R\Theta\bar{L}_T[\mathrm{Cl}]_{ld}^c \tag{46}$$

Scaling each I_{Cl}^j as usual (as in 22) but using the conductivity g_{Cl}^j appropriate to cell j, we can obtain a scale for the average current $\bar{I}_{Cl}$:

$$\bar{I}_{Cl} = \frac{z_{Cl}R\Theta}{F}\left(\frac{\sum_{i=1}^n g_{Cl}^i I_{Cl}^{i*}}{n}\right) \sim \frac{z_{Cl}R\Theta}{F}\bar{g}_{Cl} \tag{47}$$

where the last scale can be obtained by setting the individual nondimensionalized chloride currents to one. Following the same procedures as in the single-cell case to determine the $[\mathrm{Cl}]_{ld}^c$ scale (using [46] to define the relationship between $\bar{q}_a^c$ and $[\mathrm{Cl}]_{ld}^c$ scales), the appropriate isosmotic scalings are

$$\begin{aligned}[\mathrm{Cl}]_{ld}^c &= \frac{\bar{g}_{Cl}}{2\bar{L}_T[\mathrm{Cl}]_e F^2}[\mathrm{Cl}]_{ld}^{c*}, \quad \bar{I}_{Cl} = \frac{z_{Cl}\bar{g}_{Cl}R\Theta}{F}\bar{I}_{Cl}^*, \\ \bar{q}_a^c &= \frac{\bar{g}_{Cl}R\Theta}{[\mathrm{Cl}]_e F^2}\bar{q}_a^*;\end{aligned} \tag{48}$$

Using (46) to eliminate $[\mathrm{Cl}]_{ld}^c$ in (45) and substituting the scales (48) into the result, we then obtain the nondimensionalized quasi-steady-state equation:

$$\left(\frac{\bar{g}_{Cl}}{2\bar{L}_T F^2[\mathrm{Cl}]_e^2}\right)\bar{q}_a^{c*2} + \bar{q}_a^{c*} - \bar{I}_{Cl}^* = 0 \tag{49}$$

we see from this equation that a group of n lumenally coupled cells behave like (n copies of) a single cell secreting chloride at a rate equal to the average chloride secretion rate of the group. Here, we will denote the small parameter by $\alpha_c \equiv \frac{\bar{g}_{Cl}}{2\bar{L}_T F^2[\mathrm{Cl}]_e^2}$, which is the ratio of the average of the chloride-transport parameters to the average of the fluid-transport parameters (not the average of the ratio for each cell). As noted in the previous subsection, if the cells have the same water permeability, L_T, then each cell itself behaves (approximately) like a single cell secreting chloride at a rate equal to the average secretion rate of the group. The solution to this equation is analogous to the single-cell case

$$\begin{aligned}\bar{q}_a^{c*} &= \left(\frac{1}{\alpha_c}\right)\left(\frac{1}{2}\right)\left[\sqrt{1 + 4\alpha_c\bar{I}_{Cl}^*} - 1\right] \\ &= \bar{I}_{Cl}^*\left[1 - \alpha_c\bar{I}_{Cl}^* + 2\alpha_c^2\bar{I}_{Cl}^*\right] + O(\alpha_c^3)\end{aligned} \tag{50}$$

so the dimensional flow is

$$\bar{q}_a^c = \left(\frac{\bar{g}_{Cl}R\Theta}{[\mathrm{Cl}]_e F^2}\right)q_a^{c*} \equiv \bar{Q}_s^c q_a^{c*} \tag{51}$$

where $\bar{Q}_s^c \equiv \frac{\bar{g}_{Cl}R\Theta}{[\mathrm{Cl}]_e F^2} = \frac{1}{n}\sum_{i=1}^n Q_s^i$ is the scale for coupled secretion.

Coupling Effects on Efficiency

To compare the efficiency of secretion between isolated and lumenally coupled cells, we consider each cell to have a fixed chloride-secretion rate (whether coupled or not) which differs from its neighbors. We then define the efficiency of fluid secretion (in a way consistent with our single-cell analysis) as how much fluid is secreted for these fixed chloride-secretion rates for each cell. It is clear that, as in the single-cell case, the isosmotic limiting case is an upper bound on the efficiency of coupled cells.

We address the question of whether, as far as efficiency is concerned, there is any effect due to the shared lumen which goes beyond the results obtained for a single cell.

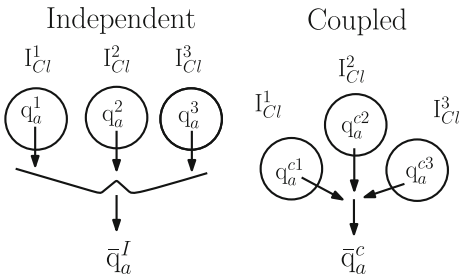

Fig. 6 Illustration of the comparison of the secretion from n independent cells to the secretion from n lumenally coupled cells, for fixed chloride currents. For simplicity, the diagram shows the case of three cells when independent compared to the same three cells (with fixed chloride currents) when lumenally coupled

Therefore, the question becomes, Is the total fluid secretion higher for n lumenally coupled cells or for n independent cells (and does this change between isosmotic and non-isosmotic regimes)? Since the number of cells is the same in each case, we can rephrase this as follows: Is the average fluid secretion higher for n lumenally coupled cells or for n independent cells (and does this change between isosmotic and nonisosmotic regimes)? This comparison is illustrated in Fig. 6. We can calculate the average fluid secretion for coupled cells using (49). The average for the uncoupled case is computed by first calculating the n independent fluid secretions for the n chloride currents and then averaging. To define this latter quantity, we first apply (35) to each independent cell j with current I_{Cl}^{j*} and transport parameters g_{Cl}^{j}, L_{T}^{j}. This gives

$$q_{\mathrm{a}}^{j} = \left(\frac{g_{\mathrm{Cl}}^{j} R\Theta}{[\mathrm{Cl}]_{\mathrm{e}} F^2}\right) q_{\mathrm{a}}^{j*} \equiv Q_{\mathrm{s}}^{j} q_{\mathrm{a}}^{j*} \tag{52}$$

for each of the dimensional fluid flows, where $Q_{\mathrm{s}}^{j} \equiv \frac{g_{\mathrm{Cl}}^{j} R\Theta}{[\mathrm{Cl}]_{\mathrm{e}} F^2}$ is the scale for the jth secretion, and

$$\begin{aligned} q_{\mathrm{a}}^{j*} &= \left(\frac{1}{\alpha_j}\right)\left(\frac{1}{2}\right)\left[\sqrt{1+4\alpha_j I_{\mathrm{Cl}}^{j*}} - 1\right] \\ &= I_{\mathrm{Cl}}^{j*}\left[1 - \alpha_j I_{\mathrm{Cl}}^{j*} + 2\alpha_j^2 I_{\mathrm{Cl}}^{j*}\right] + O(\alpha_j^3) \end{aligned} \tag{53}$$

for the nondimensional parts. We can then define the average fluid secretion for n independent cells, $\bar{q}_{\mathrm{a}}^{\mathrm{I}}$, as

$$\begin{aligned} \bar{q}_{\mathrm{a}}^{\mathrm{I}} &\equiv \frac{\sum_{\mathrm{i}=1}^{n} Q_{\mathrm{s}}^{i} q_{\mathrm{a}}^{i*}}{n} \\ &= \frac{1}{n}\sum_{i=1}^{n}\left[Q_{\mathrm{s}}^{i}\left(\frac{1}{\alpha_i}\right)\left(\frac{1}{2}\right)\left[\sqrt{1+4\alpha_i I_{\mathrm{Cl}}^{i*}} - 1\right]\right] \end{aligned} \tag{54}$$

Now, we wish to use these two expressions $\bar{q}_{\mathrm{a}}^{\mathrm{I}}$ and $\bar{q}_{\mathrm{a}}^{c}$ to compare the different average fluid secretions, i.e., to consider the difference in the average (and hence total) secretion in the coupled and independent cases. Since $q_{\mathrm{a}}^{j*} \to 1$ as $\alpha_i \to 0$ and $q_{\mathrm{a}}^{c*} \to 1$ as $\alpha_c \to 0$

$$\bar{q}_{\mathrm{a}}^{\mathrm{I}} = \frac{\sum_{\mathrm{i}=1}^{\mathrm{n}} Q_{\mathrm{s}}^{\mathrm{i}}}{n} \equiv \bar{Q}_{\mathrm{s}}^{\mathrm{c}} \equiv \frac{1}{n}\sum_{\mathrm{i}=1}^{\mathrm{n}} Q_{\mathrm{s}}^{\mathrm{i}} \qquad \text{for isosmotic secretion} \tag{55}$$

and

$$\bar{q}_{\mathrm{a}}^{c} = \bar{Q}_{\mathrm{s}}^{c} \equiv \frac{1}{n}\sum_{i=1}^{n} Q_{\mathrm{s}}^{i} \qquad \text{for isosmotic secretion} \tag{56}$$

These expressions are identical, and hence, the coupled and independent cell secretions are the same for isosmotic cases. This value is simply the average of the independent isosmotic secretions. We now wish to make the comparison in the nonisosmotic case. Since we are considering fixed chloride currents, while allowing the permeabilities to vary, we can set each of the nondimensional chloride currents to 1 so that the fixed value of each current is determined solely by its associated scaling factor. Next, we normalize each of the expressions for average fluid flow (the coupled and independent cases, respectively) relative to the shared isosmotic upper bound $\frac{\sum_{i=1}^{n} Q_{\mathrm{s}}^{i}}{n}$. These two normalized averages can then be expressed as

$$\left(\bar{q}_{\mathrm{a}}^{\mathrm{I}}\right)^{*} \equiv \frac{\bar{q}_{\mathrm{a}}^{\mathrm{I}}}{\left(\frac{\sum_{i=1}^{n} Q_{\mathrm{s}}^{i}}{n}\right)} = \frac{\sum_{k=1}^{n} Q_{\mathrm{s}}^{k} f(\alpha_k)}{\sum_{i=1}^{n} Q_{\mathrm{s}}^{i}} = \frac{\sum_{k=1}^{n} g_{\mathrm{Cl}}^{k} f\left(\frac{g_{\mathrm{Cl}}^{k}}{L_{\mathrm{T}}^{k}}\right)}{\sum_{i=1}^{n} g_{\mathrm{Cl}}^{i}} \tag{57}$$

(note this quantity is nondimensionalized as a whole since adding individually nondimensionalized quantities of the same type makes no physical sense when the scales are chosen differently—e.g., adding the numerical value of two lengths, one in centimeters and the other in meters, is physically meaningless) and

$$\bar{q}_{\mathrm{a}}^{c*} \equiv \frac{\bar{q}_{\mathrm{a}}^{c}}{\left(\frac{\sum_{i=1}^{n} Q_{\mathrm{s}}^{i}}{n}\right)} = f(\alpha_{\mathrm{c}}) \equiv f\left(\frac{\sum_{k=1}^{n} g_{\mathrm{Cl}}^{k}}{\sum_{i=1}^{n} L_{\mathrm{T}}^{i}}\right) \tag{58}$$

respectively. As mentioned, the nondimensional chloride currents are fixed at a value of 1 in the function f so that its argument is simply an α value. This function is the same as that represented in panel 2 of Fig. 2. A beneficial coupling effect on secretion will be indicated by $\bar{q}_{\mathrm{a}}^{c*} > \left(\bar{q}_{\mathrm{a}}^{\mathrm{I}}\right)^{*}$, and conversely, if $\left(\bar{q}_{\mathrm{a}}^{\mathrm{I}}\right)^{*} > \bar{q}_{\mathrm{a}}^{\mathrm{c}*}$, then coupling has a detrimental effect on total secretion. In Appendix C we show that

$$\bar{q}_{\mathrm{a}}^{c*} \geq \left(\bar{q}_{\mathrm{a}}^{\mathrm{I}}\right)^{*} \qquad \text{for non-isosmotic secretion} \tag{59}$$

follows from the convex, strictly decreasing nature of $f(\alpha)$—or, equivalently, the concave, strictly increasing nature of $F(\beta) = f\left(\frac{1}{\alpha}\right)$. Equality in (59) only holds when the α_j are all identical. Hence, in general, for nonisosmotic

secretion there is a beneficial effect on the average (and hence the total) secretion due to the lumenal coupling.

Despite the possibility of a beneficial coupling effect, the effect on secretion is never enough to make up for the difference in secretion between isosmotic and nonisosmotic regimes. As shown, the isosmotic case is an upper bound for both coupled and uncoupled secretion. Since the coupling effect is mathematically due to the convexity (concavity) of the function $f(\alpha)$ $(F(\beta))$, we expect the effect to be greater for greater ranges of α (β) values (for small ranges any differentiate function is close to linear). Thus, this coupling benefit plays an essentially compensatory role for deviations from normal function—a positive coupling effect requires nonisosmotic secretion and a significant spread in parameter values. We can summarize these results with the ordering isosmotic independent = isosmotic coupled > nonisosmotic coupled > nonisosmotic independent, where the ordering is with respect to efficiency.

This does not quite complete the analysis, however, since we have compared cases at fixed chloride currents. As mentioned, it may be the case that coupling significantly modifies the chloride currents; i.e., a coupled arrangement may have a higher or lower total fluid secretion than that calculated for fixed chloride currents if the average chloride current increases or decreases due to interactions via the shared lumen. We can easily rule this out in the isosmotic case—although the fluid-secretion rates change when coupled (to close to a common rate as shown in the previous section), we would expect no change in the chloride secretion. The difference between the two is that the fluid secretion depends very sensitively on small changes in lumenal concentrations due to the large permeability, while changes in chloride secretion require much larger lumenal changes for non-negligible effects. Since, by assumption, in the isosmotic case all changes in the lumen are negligible, the cells do not "see" each other via the lumen and, thus, each cell continues to secrete chloride as it did before.

The nonisosmotic case is not so straightforward—although it may be reasonable to simply assume the average chloride current will not change significantly when cells are coupled (although some individual currents may go up or down), it depends on the details of the model. To check the reasonableness of this assumption and to verify some of our results obtained so far, we turn next to simulation.

Simulations

As in the single-cell case, we now validate and extend the analysis we have undertaken by considering a particular model with specific flux equations, signaling dynamics and parameters, allowing model simulation. Each cell in the multicell simulation is identical (other than initial conditions and/or "stimulation parameter" v) to that discussed in the single-cell case. For simplicity of presentation, we illustrate the results here with the case of three cells; however, the results hold for any number.

Individual Secretions

Figure 7 illustrates the individual secretions from differently stimulated cells in an acinus arrangement. The choices of stimulation parameter (v, the maximum rate of IP_3 production) correspond to a representative range between the minimum and maximum values used by Palk et al. (2010) in their calcium model. The details here are unimportant; essentially, higher parameter choices correspond to a more stimulated cell. Although each cell is stimulated differently and has different chloride and sodium currents from each cell as well as different ion levels, we see that, consistent with our analysis, the fluid secretions change and are close to identical in this case. The two more highly stimulated cells each have decreases in their time-averaged fluid secretion rate of between 12 and 13% when lumenally coupled compared to their secretion rates when uncoupled, while the cell with the lower stimulation has an increase in secretion of about 25%. In accordance with the discussion of efficiency, the effect on total secretion appears to be small, if any. In the subsection following the next, we consider whether there are any coupling effects on chloride currents, and hence fluid secretion, as the permeability is decreased and lumenal concentrations increase.

Efficiency of Secretion

As in the single-cell case, simulations verify that a change in efficiency for different sizes of concentration gradient

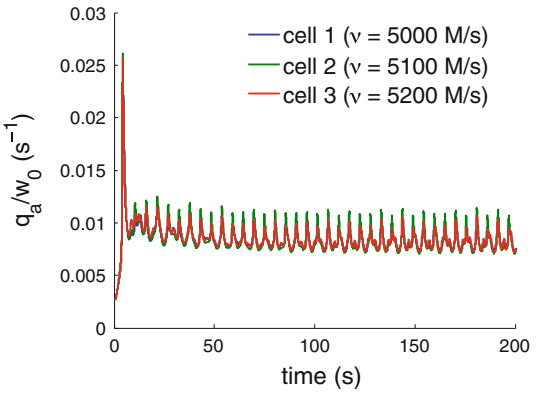

Fig. 7 Individual secretions from differently stimulated cells. Each cell is stimulated differently, but, due to the shared lumen, they secrete saliva at close to the same rate. $L_{pa} = 1.23 \times 10^{-14}$ L^2 J^{-1} s^{-1} and $L_{pb} = 4L_{pa}$ in all cases

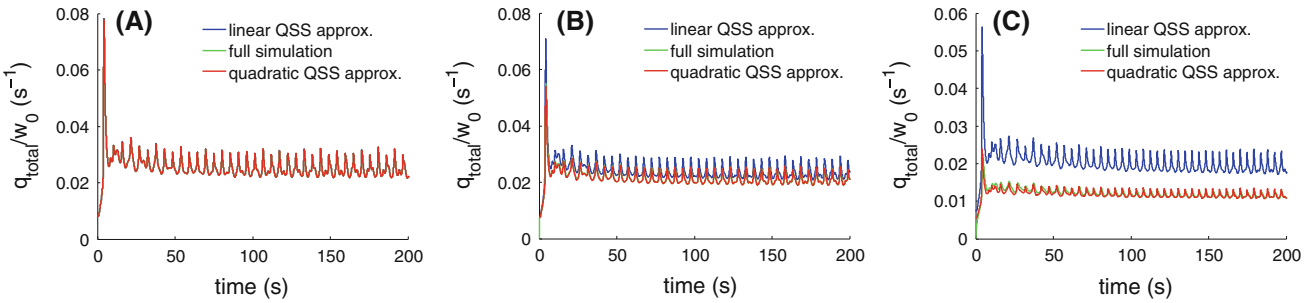

Fig. 8 Efficiency of total secretion under coupled conditions. **a** $L_{pa} = 1.23 \times 10^{-14}$ L^2 J^{-1} s^{-1}. **b** $L_{pa} = 1.23 \times 10^{-16}$ L^2 J^{-1} s^{-1}. **c** $L_{pa} = 1.23 \times 10^{-17}$ L^2 J^{-1} s^{-1}. $L_{pb} = 4L_{pa}$ in all cases

accounts for the majority of changes in total fluid secretion under coupled conditions (Fig. 8). Each cell still secretes at close to a common rate (not shown), but this common rate decreases away from the isosmotic regime, accounting for the reduction in total secretion. During rapid spikes, the difference between the quadratic quasi-steady state and the actual simulations for lower permeability values appears less than in the single-cell case; however, this is due to each cell being stimulated differently—some cells are oscillating less than they would be for the typical v value (the calcium oscillations decrease either side of the typical stimulation value). When each cell is stimulated at the same, typical, value (producing the largest oscillations) the actual secretion again fails to full reach the quasi-steady-state value during rapid spikes, for lower-permeability cases.

Secretion from an Acinus Versus Independent Secretion

Finally, we consider comparisons between coupled and uncoupled cells. As discussed previously, it is relatively easy to compare fluid secretions analytically at fixed chloride currents to analyze efficiency. Whether or not there is any net change due to a change in average or total chloride secretion, e.g., is a harder question and depends on the model details chosen. Figure 9 shows comparisons between independent cells and coupled cells for a range of permeabilities (i.e., for secretion under different conditions, isosmotic/high permeability and nonisosmotic/lower permeability). From these simulations, we see that, as predicted, the total fluid secretion is identical under isosmotic conditions, while there are small but essentially negligible changes in the total fluid secretion under non-isosmotic conditions, even though the individual secretions change to a common rate. For the model chosen the average chloride current did not show any significant differences between the coupled and uncoupled cases, though there was a small (around 1%) decrease in average current between coupled and uncoupled cases, for the lower-permeability values. The range of chloride currents—a range

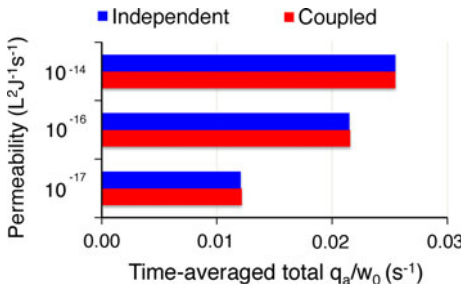

Fig. 9 Comparison of the time-averaged total secretion from independent and coupled cells for a range of permeabilities. *Top group* $L_{pa} = 1.23 \times 10^{-14}$ L^2 J^{-1} s^{-1}. *Middle group* $L_{pa} = 1.23 \times 10^{-16}$ L^2 J^{-1} s^{-1}. *Bottom group* $L_{pa} = 1.23 \times 10^{-17}$ L^2 J^{-1} s^{-1}. $L_{pb} = 4L_{pa}$ in all cases

of about 23% of the current at normal stimulation—means that the convexity/concavity effects are not expected to be large. This, combined with the negligible decrease in total current, means that only a negligible coupling effect of any sort is observed on total secretion. Thus, under typical parameter variations, we do not expect non-negligible lumenal-coupling effects.

Discussion

Recent models of salivary secretion, e.g., those of Gin et al. (2007) and Palk et al. (2010), are relatively easy to simulate using appropriate computational tools; but it can be difficult to understand the results in a simple manner. Weinstein and Stephenson (1979, 1981a, b) combined analysis of a high-level model of a single neutral solute with more comprehensive simulation models in a particularly careful and insightful manner. The work we have presented follows in this spirit by focusing on key general features of water transport, combining both approximate analysis and simulations. We have focused attention on a physiologically detailed, dynamic saliva-secretion model. Most of the prior work has placed more emphasis on fluid absorption, often from a small compartment into a larger compartment;

and the analytic work has focused on steady-state conditions, as opposed to quasi-steady-state conditions. Furthermore, most of the prior analytic work considers linearizations/perturbation expansions about isotonic/isosmotic conditions. In the context of saliva secretion into a small lumenal space, we have considered conditions for, and deviations from, quasi-steady-state conditions, deviations from isotonic/isosmotic secretion as well as effects of lumenal coupling. The main physiological application we discuss here, beyond consideration of conditions for isotonic/isosmotic secretion discussed in the next subsection, is to the interpretation of, and debate surrounding, aquaporin knockout studies, discussed below.

Isotonic/Isosmotic Water Transport: Relationship to Previous Studies

A consistent theme in discussion about fluid transport in epithelia is how isotonic/isosmotic water transport is achieved. The most commonly accepted view is that water follows salt secretion osmotically, and this, combined with relatively large water permeabilities (due to the presence of aquaporins), is sufficient to account for the basic phenomenon of saliva secretion (Spring 1999). As discussed by Turner and Sugiya (2002), one of the main problems with this hypothesis is that it is very difficult to demonstrate the existence of osmotic gradients between the interstitium and lumen. However, due to the high water permeability, it is supposed that only very small gradients are required (Spring 1999), so this becomes a problem of verifiability rather than an inconsistency with the hypothesis itself. Other evidence, in particular that based on aquaporin knockout studies (e.g., Ma et al. 1999), is usually taken to weight the evidence in favor of the osmotic hypothesis. However, the interpretation of these knockout studies has been criticized by researchers such as Hill et al. (2004) and Fischbarg (2010). We discuss this further below.

Our model is a compartment model based on an osmotic coupling mechanism. In terms of the original Curran (1960) model for epithelial transport, mapped onto the physiology of saliva secretion, the lumen plays the role of the "middle" compartment for the secretion out of the cell, though the cell itself also draws water through the basolateral membrane. Friedman (2008) offers a good discussion of how the Curran (1960) model can be used as the basic model for various physiological systems. Weinstein and Stephenson (1979, 1981a, b) emphasized a number of important distinctions relevant to key questions of epithelial transport, in particular the different parameter and boundary condition dependencies of the cases of approximate isotonicity and exact isotonicity/uphill transport. Similarly, Mathias and Wang (2005) presented a series of simple theoretical models, also based on the Curran (1960) compartment model, to investigate conditions for the generation of isotonic water transport using the osmotic mechanism. They analyzed two variations of a simple two-membrane steady-state model, one without an imposed boundary condition on the secretion (i.e., the osmolarity of the secretion is determined from the balance of salt and water transport) and one with an imposed boundary condition, setting the osmolarity to be exactly equal at each end. Due to the large permeabilities, the model behavior has a strong dependence on the selection of boundary conditions. This observation is consistent with the earlier work of Weinstein and Stephenson (1979, 1981a, b).

The first case considered by Mathias and Wang (2005) is most appropriate for models of saliva secretion due to our assumption of no pressure buildup in the lumen of a secretory end piece; i.e., any saliva previously secreted is pushed out of the lumen by newly secreted saliva (and then travels through a system of ducts before exiting into the mouth). This corresponds to the case discussed by Weinstein and Stephenson (1979, 1981a, b) of transport into a small serosal bath from a larger mucosal bath (which they discuss in reference to a hanging gallbladder experimental arrangement). For saliva secretion, this means that concentrations in the lumen are determined by a balance of salt and water transport. This is consistent with recent models published for saliva secretion (Gin et al. 2007; Palk et al. 2010).

These single-cell models of saliva secretion explicitly account for changes over time (i.e., are dynamic models), while the cells are modeled as well mixed. The model of Mathias and Wang (2005) does not include time, and in the case of interest, the spatial gradients are negligible. Weinstein and Stephenson (1979, 1981a, b) include some dynamics in their simulation model, but their corresponding theoretical treatment focuses on steady states (as opposed to quasi-steady states). Our analysis of the Gin et al. (2007) model of saliva secretion from a parotid acinar cell allows us to consider how (linearized/perturbation) analysis such as that of Mathias and Wang (2005) and those of Weinstein and Stephenson (1979, 1981a, b) carries over to a dynamic, physiologically based model of fluid secretion, regulated by an oscillating calcium signal. Our analysis shows that a large membrane permeability (relative to chloride conductivity) both is required for and leads to isosmotic secretion for osmotically driven saliva secretion. The scale of small deviations from iso-osmolarity is shown to be inversely proportional to the membrane permeability and proportional to the ratio of chloride-transport and fluid-transport terms. Furthermore, the case of isosmotic secretion provides an upper bound on saliva secretion efficiency for both single cells and cells arranged in an acinus. These results are in agreement with the work of the

aforementioned authors in their particular models. As discussed in Gin et al. (2007) and Palk et al. (2010), the basic model used here is in good agreement with estimates of total saliva secretion and of other quantities of interest such as membrane potential.

Aquaporin Knockout Studies

Overview

Hill et al. (2004) and Fischbarg (2010) (among others) have criticized the usual interpretation of aquaporin knockout studies in the context of epithelial fluid transport. In particular they focus on the fact that, in aquaporin knockout animals, water permeability is often reduced by a larger proportion than is the water transport. Although some studies, such as that of aquaporin-5-deficient mice by Krane et al. (2001), do not appear to suffer this issue, we will consider the more extreme cases of apparent conflict from a general point of view informed by our modeling work and give a representative quantitative comparison to the results of Ma et al. (1999) for aquaporin-5 knockout mice, as they are summarized in Hill et al. (2004). This requires consideration of cases for which the osmotic gradients become more significant than can be appropriately treated with a perturbation expansion near the isotonic/isosmotic secretion regime.

Hill et al. (2004) emphasize two interconnected points in their critique of the "simple permeability hypothesis" (SPH, the hypothesis being that the main role of aquaporins is to provide a path of increased water permeability to increase water transport). This hypothesis plays a crucial role in providing the large permeabilities required for the osmotic mechanism. The first, and main, point the authors raise is that the differing magnitudes of the reduction of permeability, on the one hand, and the reduction of water transport, on the other, raises problems for this hypothesis—as they say, "SPH would predict that the removal of a major pathway of water flux across membranes would have drastic effects on biological function at the cellular, tissue and whole animal level" (Hill et al. 2004, p. 8), and "where fluid flow has been significantly reduced… it has only been partial where it should have been substantial" (p. 11). The second point they raise is that there often appears to be a reduction in the total salt transport, which would by itself be enough to account for a significant portion of the reduction in fluid transport, without leaving much to be accounted for by the reduced water permeability. Though they acknowledge that their calculation of the reduction in salt transport is complicated by the possibility of changes in ductal absorption, the point remains that any reduction in salt transport leaves less reduction in fluid transport to be directly attributable to the decreased membrane permeabilities. Thus, the overall point raised is that large reductions in water permeability due to aquaporin knockouts do not appear to be having a significant enough effect on water-transport rates. Representative changes cited by Hill et al. (2004) are around 40–60% for both fluid and salt transport and up to 90% for membrane permeability, although these vary across the range of studies they consider.

Here, we consider whether such changes really are inconsistent with a model such as ours, which is based on the SPH and the corresponding osmotic mechanism for saliva secretion. Quantitative comparisons of model and experiment are discussed in the following subsection; however, we first note that according to the relationship (35) (illustrated in Fig. 2), a drop in fluid transport essentially has two components—one due to a decrease in the chloride current and one due to a drop in efficiency (i.e., when permeability is lowered and the osmotic gradient increased). As the isosmotic regime is approached (the large permeability limit), these effects become essentially independent. Furthermore, as this regime is approached, the fluid transport loses all dependence on permeability—the dependence disappears according to an inverse relationship in permeability (since $\alpha \sim 1/L_T$). So when the physiological system is in this parameter range, a drop in chloride current is associated with a direct linear decrease in fluid transport, while a significant drop in permeability may not have much effect at all. As long as the ratio of chloride conductance to water permeability is sufficiently small, the system will remain in this regime. Thus, the role of aquaporins may be not only to increase the fluid transported for a given amount of salt transport but also to push the system into a regime where it is more robust to variations in permeability.

Comparison to Experiments

The water permeability used in the simulation shown in Fig. 4c is an order of magnitude lower than the water permeability used in the simulation shown in Fig. 4b. This corresponds to a drop in water permeability of 90%. At the same time, the drop in fluid flow (here denoted by J_v instead of q_a) is only about 51%. A comparison of these results with those of Ma et al. (1999) as summarized by Hill et al. (2004) is given in Table 1. As can be seen, these results are of a similar scale to those of Ma et al. (1999), which Hill et al. (2004) cite as being in conflict with the SPH. In particular, the large drop in water permeability (of 90%) produces a much less marked drop in fluid secretion (51% in the model, 59% observed experimentally), along with a drop in convective salt collection rate (J_s) (27% compared to 41% observed experimentally). It is apparent that a large reduction in water permeability is not

Table 1 Comparison of aquaporin knockout studies and representative model dependence on water permeability

Knockout				Model				
ΔPosm	ΔJ_v	ΔOsm	ΔJ_s	ΔPosm	ΔJ_v	ΔOsm	ΔJ_s	ΔI_{Cl}
−65 to −90%[a]	−59%	+43%	−41%	−90%	−51%	+41%	−27%	−19%

Data are from Ma et al. (1999) and include an estimate of J_v changes as calculated by Hill et al. (2004)

[a] Ma et al. (1999) did not measure the decrease in cell membrane permeability in their knockout experiment. Krane et al. (2001) found a relative decrease in permeability (as measured by changes in swelling/shrinking rates) in aquaporin-knockout mice of 65% for parotid and 77% for sublingual cells. Aquaporins are estimated to account for up to 90% of cell water permeability in various physiological systems, as summarized by Hill et al. (2004)

inconsistent with a smaller reduction in fluid secretion, according to results produced entirely according to the SPH mechanism. The drop in (measured) salt transport is also largely accounted for, and actually corresponds to a much lower decrease in the chloride current (I_{Cl}) itself (19%), due to deviations from quasi-steady-state behavior (as discussed above, Numerical Simulations). Further decreases in chloride-transport rates not accounted for in the model could be due to changes in duct absorption rates in knockouts (affecting J_s) or other changes in cell chloride secretion (affecting I_{Cl} and J_s) in knockouts.

The effect of a 99% permeability decrease on water transport is even less going from Fig. 4a, b as these are further in the isosmotic parameter range, and hence, the results are even less susceptible to variations in permeability. The water permeability values used here were originally model fits by Gin et al. (2007), and the largest value used is probably one to two orders of magnitude too large, based on the range for typical epithelia (Spring 2010). The exact membrane water permeabilities are difficult to measure in glandular acini (Hill et al. 2004), and we are not aware of any values for parotid glands in the literature. However, in our representative comparison with aquaporin studies given above we used a baseline permeability of two orders of magnitude less than that of Gin et al. (2007) (Fig. 4b) and then considered a further order of magnitude decrease (Fig. 4c), consistent with the expected range of permeability values (we present a conversion from our units for water permeability to an equivalent P_f value in Appendix A). Based on our results (including those given below), we would expect the permeability of parotid acinar cells to be similar to that of other high-permeability cells in other water-transporting epithelia such as the lung (Dobbs et al. 1998) and renal proximal tubule (Meyer and Verkman 1987), i.e., a P_f of the order 10^{-2} cm s^{-1}.

Acinus Geometry

Mathematical models of saliva secretion (e.g., Gin et al. 2007; Palk et al. 2010) have so far focused on single cells. However, in this analysis we have begun to consider the effects of acinus geometry on secretion. In particular, we considered the coupling effect induced by the shared lumen of an acinus on the dynamics of the cells making up that acinus. We demonstrated how to carry over the results for efficiency and isosmotic/nonisosmotic secretion to this case. Furthermore, we illustrated two key points. Firstly, the individual fluid secretions of member cells in an acinus are in fact modified by the arrangement of the cells around a single shared lumen. Differently stimulated cells can secrete fluid at close to identical rates when arranged into an acinus, while this is not the case for isolated cells. However, the total fluid secreted from an acinus is not affected by this lumenal coupling. It is worth noting that in real salivary glands the lumenal structure can be more convoluted and is continuous with intercellular canaliculi (Riva et al. 1993).

Calcium Signaling

In this work we included an oscillating calcium signal which, e.g., leads to deviations from (quasi-) steady-state behavior. We have not considered effects of the acinus geometry on this calcium signaling. Work in progress includes, from the single-cell perspective, incorporating calcium waves (originating at the apical end) to explore the observation of the relatively rapid calcium wave speed (e.g. compared to that in the pancreas [Giovannucci et al. 2002]) in the context of the type of signaling that works best for fluid secretion. In the multicellular case, work has begun to explore the effects of the inclusion of gap junctions on calcium signaling and hence fluid secretion. In each of these cases, the analysis of the salt and water coupling effects carried out here forms a foundation from which to consider these extensions. The effects of variations in calcium signaling, in both a single cell and an acinus, can profit from the reduction in complexity of the fluid secretion model, e.g., utilizing the simple relations derived between fluid secreted and chloride current. Changes in transporters and ionic mechanisms can also be understood using modifications of the analysis carried out here.

Transport Routes and Ionic Mechanisms

The chloride-based mechanism adopted in this report is thought to account for the majority of saliva secretion from the major salivary glands. But it is also thought possible that bicarbonate exits the cell via the same apical anion channel as chloride (Turner and Sugiya 2002), and we have not represented this mechanism in our model. There may be interesting consequences of including this additional mechanism; however, the essential feature of anion secretion via the apical membrane and cation flow via the tight junctions (establishing an osmotic gradient in the lumen) is the same. Since the water secretion into the lumen washes all ions away, in principle there must be a bicarbonate current into the lumen; here, it is essentially assumed that it would in reality make up some fraction of the total apical anion current into the lumen, which for the same osmotic gradient would mean a slightly lower chloride current than is present in this model. The proper inclusion of bicarbonate in the model remains future work, as does the inclusion of details from other suggested ionic mechanisms (Turner and Sugiya 2002; Cook and Young 2010).

The effect on secretion of a possible apical K^+ channel was considered by Cook and Young (1989) and more recently by Palk et al. (2010). While our analysis could be extended to cover this, it is beyond the scope of the present study. In our model Na^+ and K^+ travel only via the paracellular pathway, which is assumed to be cation-selective in accordance with the basic proposed mechanisms of saliva secretion (Cook and Young 2010). In general, these ionic fluxes will be driven by their electrochemical gradients, as well as by convection by any water traveling via this same pathway. We ignore direct ion–ion interactions; however, if solute reflectivities differ between two (or more) parallel pathways (e.g., the paracellular pathway and the cell) through which water also travels, then cross-terms in overall (or "composite") epithelium system equations can still occur. These represent formal ion–ion interactions and can have important consequences for the interpretation of tracer flux experiments and the determination of permeabilities (Weinstein 1987). Since in our model we assume a fully transcellular pathway for water (consistent with the assumption of an osmotic mechanism as discussed in the Introduction), these formal composite-system interactions are not present (Weinstein 1987; Friedman 2008).

Despite this, it still may be of interest to consider a paracellular water flux, via either an osmotic mechanism or some other mechanism, to better clarify and understand the model dependence on this assumption and the consequences for determining parameter values experimentally. Gin et al. (2007) and Palk et al. (2010) both considered a paracellular water flux; however, they did not consider an explicit convective solute flux (or any other similar paracellular flux coupling, as can be formalized using the framework of nonequilibrium thermodynamics [Schultz 1980]). Without this, they found no qualitative differences in model behavior. This can be explained by the expression we derived for the secretion from a cell (32) (which applies for both isolated cells and cells in an acinus), which is dependent only on the lumenal and interstitial concentrations and thus has the same form as a simple paracellular flux. Finally, we note that the specific equations representing the paracellular ion fluxes will change depending on the included mechanisms, but the electroneutrality equation that we use (11) holds (approximately) regardless of the mechanism of ion flux.

Acknowledgement We thank Ted Begenisich, David Yule and Trevor Shuttleworth at the University of Rochester; James Melvin and Marcelo Catalan at the National Institutes of Health (NIH); and Laurence Palk, Kate Patterson, Katie Sharp, Shawn Means, Ivo Siekmann and Vivien Kirk from the University of Auckland for helpful discussions and feedback. We also thank the anonymous referees for detailed and helpful comments that we feel significantly improved this work. O. M. was supported by the Tertiary Education Commission's Top Achiever Doctoral Scholarship. This work was supported by NIH grant R01 DE19245-01.

Appendix A: Water Permeability

We have used the units $L^2\ J^{-1}\ s^{-1}$ for water permeability, in line with Palk et al. (2010) and which we found convenient for simulation and analysis but which are not as common among physiologists. A variety of quantities characterizing water permeability are in use in epithelial water-transport studies; here, we give a conversion from our water permeability to an equivalent P_f ("osmotic water permeability") quantity, which is measured in centimeters per second.

We first note that our permeability is an area-weighted quantity, as employed by Gin et al. (2007) and Palk et al. (2010). We use the data from Cope and Williams (1974) and Poulsen and Bundgaard (1994) to give a typical value for apical membrane area of about $A = 1.25 \times 10^{-6}$ cm^2. The remaining quantities required for conversion are $R = 8.315$ J mol^{-1} K^{-1}, $\Theta = 310$ K, $V_w = 18 \times 10^{-3}$ L mol^{-1} and 10^3 cm^3 $= 1$ L. The relationship between our L_{pa} and the quantity P_f, expressed using these quantities, is (Persson and Spring 1982)

$$P_f = \frac{10^3 R\Theta L_{pa}}{A V_w} \tag{60}$$

where 10^3 is a conversion factor for $\frac{L_{pa}}{V_w}$ (the ratio of which has units L mol J^{-1} s^{-1}) from liters to centimeters cubed. This gives an equivalent value for P_f of about 1.41 cm s^{-1} for our highest permeability ($L_{pa} = 1.23 \times 10^{-14}$ L^2 J^{-1} s^{-1}) and a value of about 1.41×10^{-2} cm s^{-1} for the

value we take as representative in our comparisons to aquaporin knockout studies ($L_{pa} = 1.23 \times 10^{-16}$ L^2 J^{-1} s^{-1}). This latter value is similar to those of other water-transporting epithelia, as discussed in the main text, while the higher value represents a limiting case.

Appendix B: Calcium Signaling Model Modification

As noted by Palk et al. (2010), the Gin et al. (2007) model appeared to have a dependence of calcium oscillations on volume oscillations, which they deemed undesirable. Because of this, our calcium model follows that of Palk et al. (2010). The only difference is that our model uses a Hill function expression for IP_3 production

$$J_{\text{IP3prod}} = v_{w_0} \frac{[\text{Ca}]_i^2}{[\text{Ca}]_i^2 + \text{K}^2} \tag{61}$$

where K = 5 nM and v is a control parameter with a typical value of 5,100 M s^{-1}, while their model has a constant production rate:

$$J_{\text{IP3prod}} = v_{w_0} \tag{62}$$

This makes no difference to the results. The rest of the signaling model is identical and follows the details given in their paper (see pp. 626–628 and Tables 1–3).

Appendix C: Beneficial Coupling Effect

Function Properties

We state without proof that, for $\alpha \in [0, \infty)$, the function $f(\alpha) = \left(\frac{1}{\alpha}\right)\left(\frac{1}{2}\right)\left[\sqrt{1+4\alpha} - 1\right]$ is (1a) convex and (2a) strictly decreasing. We define the value at $\alpha = 0$ to be the limit as $\alpha \to 0$, which exists and is equal to 1. Defining the new variable $\beta = 1/\alpha$, we can define the new function:

$$F(\beta) = (\beta)\left(\frac{1}{2}\right)\left[\sqrt{1+4\left(\frac{1}{\beta}\right)} - 1\right] = f(1/\beta)$$

Over $\beta \in [0, \infty)$, this function is (1b) concave and (2b) strictly increasing. We again state this without proof. However, these function properties can be verified simply, by plotting the functions (for positive values) along with the first and second derivatives. A negative (positive) first derivative indicates a decreasing (increasing) function, and a positive (negative) second derivative indicates a convex (concave) function. The freely available computational tool Wolfram Alpha (www.wolframalpha.com), e.g., can be used. This can compute the derivatives and handle the singularity at zero automatically.

Positive Coupling Effect

Now we can write (57) and (58) (derived for fixed chloride currents) as

$$\left(\bar{q}_a^{\text{I}}\right)^* = \frac{\sum_{k=1}^n g_{\text{Cl}}^k F\left(\frac{L_T^k}{g_{\text{Cl}}^k}\right)}{\sum_{i=1}^n g_{\text{Cl}}^i} \tag{63}$$

and

$$\bar{q}_a^{c*} = F\left(\frac{\sum_{k=1}^n L_T^k}{\sum_{i=1}^n g_{\text{Cl}}^i}\right) = F\left(\sum_{k=1}^n \frac{g_{\text{Cl}}^k \left(\frac{L_T^k}{g_{\text{Cl}}^k}\right)}{\sum_{i=1}^n g_{\text{Cl}}^i}\right) \tag{64}$$

Thus, (63) is a weighted average of F evaluated at each $\left(\frac{L_T^j}{g_{\text{Cl}}^j}\right)$ value, while (64) is equal to F evaluated at the weighted average of the $\left(\frac{L_T^j}{g_{\text{Cl}}^j}\right)$ values. By Jensen's inequality (Hardy et al. 1997) applied to concave, strictly increasing $F\left(\frac{L_T^j}{g_{\text{Cl}}^j}\right)$, it follows that

$$\bar{q}_a^{c*} \geq \left(\bar{q}_a^{\text{I}}\right)^* \tag{65}$$

where the inequality is strict when the $\left(\frac{L_T^j}{g_{\text{Cl}}^j}\right)$ values are not all identical. This gives the required result.

References

Arreola J, Melvin JE, Begenisich T (1996) Activation of calcium-dependent chloride channels in rat parotid acinar cells. J Gen Physiol 108:35–47

Benjamin BA, Johnson EA (1997) A quantitative description of the Na–K–2Cl cotransporter and its conformity to experimental data. Am J Physiol 273:F473–F482

Cook DI, Young JA (1989) Effect of K^+ channels in the apical plasma membrane on epithelial secretion based on secondary active Cl^- transport. J Membr Biol 110:139–146

Cook DI, Young JA (2010) Fluid and electrolyte secretion by salivary glands. In comprehensive physiology. John Wiley & Sons, Hoboken

Cope GH, Williams MA (1974) Improved preservation of parotid tissue for electron microscopy: a method permitting the collection of valid stereological data. J Cell Biol 60(1):292–297

Curran PF (1960) Na, Cl, and water transport by rat ileum in vitro. J Gen Physiol 43:1137–1148

Diamond JM (1964) The mechanism of isotonic water transport. J Gen Physiol 48:15–42

Diamond JM, Bossert WH (1967) Standing-gradient osmotic flow. J Gen Physiol 50(8):2061–2083

Dobbs LG, Gonzalez R, Matthay MA, Carter EP, Allen L, Verkman AS (1998) Highly water-permeable type I alveolar epithelial cells confer high water permeability between the airspace and vasculature in rat lung. Proc Natl Acad Sci USA 95:2991–2996

Fischbarg J (2010) Fluid transport across leaky epithelia: central role of the tight junction and supporting role of aquaporins. Physiol Rev 90:1271–1290

Friedman M (2008) Principles and models of biological transport. Springer, New York

Gin E, Crampin EJ, Brown DA, Shuttleworth TJ, Yule DI, Sneyd J (2007) A mathematical model of fluid secretion from a parotid acinar cells. J Theor Biol 248:64–80

Giovannucci DR, Bruce JIE, Straub SV, Arreola J, Sneyd J, Shuttleworth TJ, Yule DI (2002) Cytosolic Ca^{2+} and Ca^{2+}-activated Cl^{-} current dynamics: insights from two functionally distinct mouse exocrine cells. J Physiol 540(2):469–484

Hardy G, Littlewood J, Polya G (1997) Inequalities. Cambridge mathematical library. Cambridge University Press, Cambridge

Hill AE (2008) Fluid transport: a guide for the perplexed. J Membr Biol 223(1):1–11

Hill AE, Hill BS (1978) Sucrose fluxes and junctional water flow across *Necturus* gall bladder epithelium. Proc R Soc Lond B 200(1139):163–174

Hill AE, Shachar-Hill B, Shachar-Hill Y (2004) What are aquaporins for? J Membr Biol 197:1–32

Krane CM, Melvin JE, Nguyen HV, Richardson L, Towne JE, Doetschman T, Menon AG (2001) Salivary acinar cells from aquaporin 5-deficient mice have decreased membrane water permeability and altered cell volume regulation. J Biol Chem 276:23413–23420

Krantz W (2007) Scaling analysis in modeling transport and reaction processes: a systematic approach to model building and the art of approximation. Wiley-Interscience, Hoboken

Läuger P, Apell HJ (1986) A microscopic model for the current–voltage behaviour of the Na, K-pump. Eur Biophys 13:309–321

Lytle C, McManus T (1986) A minimal kinetic model of Na^{+} K^{+} 2Cl co-transport with ordered binding and glide symmetry. J Gen Physiol 88:36a

Ma T, Song Y, Gillespie A, Carlson EJ, Epstein CJ, Verkman AS (1999) Defective secretion of saliva in transgenic mice lacking aquaporin-5 water channels. J Biol Chem 274(29):20071–20074

Mathias RT, Wang H (2005) Local osmosis and isotonic transport. J Membr Biol 208:39–53

Meyer MM, Verkman AS (1987) Evidence for water channels in renal proximal tubule cell membranes. J Membr Biol 96:107–119

Palk L, Sneyd J, Shuttleworth TJ, Yule DI, Crampin EJ (2010) A dynamic model of saliva secretion. J Theor Biol 266(4):625–640

Persson BE, Spring KR (1982) Gallbladder epithelial cell hydraulic water permeability and volume regulation. J Gen Physiol 79:481–505

Poulsen JH, Bundgaard M (1994) Quantitative estimation of the area of luminal and basolateral membranes of rat parotid acinar cells: some physiological applications. Pflugers Arch 429(2):240–244

Riva A, Valentino L, Lantini MS, Floris A, Riva FT (1993) 3D structure of cells of human salivary glands as seen by SEM. Microsc Res Tech 26(1):5–20

Schultz S (1980) Basic principles of membrane transport. IUPAB biophysics series. Cambridge University Press, Cambridge

Schultz SG (2001) Epithelial water absorption: osmosis or cotransport? Proc Natl Acad Sci USA 98:3628–3630

Segel LA (1970) Standing-gradient flows driven by active solute transport. J Theor Biol 29(2):233–250

Segel LA (1972) Simplification and scaling. SIAM Rev 14(4): 547–571

Segel L, Goldbeter A (1994) Scaling in biochemical kinetics: dissection of a relaxation oscillator. J Math Biol 32:147–160

Segel LA, Slemrod M (1989) The quasi-steady-state assumption: a case study in perturbation. SIAM Rev 31(3):446–477

Shachar-Hill B, Hill AE (2002) Paracellular fluid transport by epithelia. In: Thomas Zeuthen WDS (ed) Molecular mechanisms of water transport across biological membranes. International review of cytology, vol 215. Academic Press, San Diego, pp 319–350

Smith NP, Crampin EJ (2004) Development of models of active ion transport for whole-cell modeling: cardiac sodium-potassium pump as a case study. Prog Biophys Mol Biol 85:387–405

Spring KR (1998) Routes and mechanism of fluid transport by epithelia. Annu Rev Physiol 60:105–119

Spring KR (1999) Epithelial fluid transport—a century of investigation. News Physiol Sci 14(3):92–98

Spring KR (2010) Mechanism of fluid transport by epithelia. John Wiley & Sons, Hoboken

Takahata T, Hayashi M, Ishikawa T (2003) SK4/IK1-like channels mediate TEA-insensitive, Ca^{2+}-activated K^{+} currents in bovine parotid acinar cells. Am J Physiol 284:C127–C144

Thaysen JH, Thorn NA, Schwartz IL (1954) Excretion of sodium, potassium, chloride and carbon dioxide in human parotid saliva. Am J Physiol 178(1):155–159

Turner RJ, Sugiya H (2002) Understanding salivary fluid and protein secretion. Oral Dis 8:3–11

Turner RJ, Paulais M, Manganel M, Lee SI, Moran A, Melvin JE (1993) Ion and water transport mechanisms in salivary glands. Crit Rev Oral Biol Med 4:385–391

Weinstein AM (1987) Convective paracellular solute flux. A source of ion–ion interaction in the epithelial transport equations. J Gen Physiol 89:501–518

Weinstein AM, Stephenson JL (1979) Electrolyte transport across a simple epithelium. Steady-state and transient analysis. Biophys J 27(2):165–186

Weinstein AM, Stephenson JL (1981a) Coupled water transport in standing gradient models of the lateral intercellular space. Biophys J 35(1):167–191

Weinstein AM, Stephenson JL (1981b) Models of coupled salt and water transport across leaky epithelia. J Membr Biol 60:1–20